

Conductivity of the holographic p -wave superconductors with higher order corrections

Mahya Mohammadi^{1,*} and Ahmad Sheykhi^{1,2,†}

¹*Physics Department and Biruni Observatory, Shiraz University, Shiraz 71454, Iran*

²*Research Institute for Astronomy and Astrophysics of Maragha (RIAAM), P. O. Box: 55134-441, Maragha, Iran*

We investigate the holographic p -wave superconductors in the presence of the higher order corrections on the gravity as well as on the gauge field side. On the gravity side, we add the Gauss-Bonnet curvature correction terms, while on the gauge field side we take the nonlinear Lagrangian in the form $\mathcal{F} + b\mathcal{F}^2$, where \mathcal{F} is the Maxwell Lagrangian and b indicates the strength of nonlinearity. We employ the shooting method for the numerical calculations in order to obtain the ratio of the critical temperature T_c over $\rho^{1/(d-2)}$. We observe that by increasing the values of the mass and the nonlinear parameters the critical temperature decreases and thus the condensation becomes harder to form. In addition, the stronger Gauss-Bonnet parameter α hinders the superconducting phase in Gauss-Bonnet gravity. Furthermore, we calculate the electrical conductivity based on the holographic setup. The real and imaginary parts are related to each other by Kramers-Kronig relation which indicates a delta function and pole in low frequency regime, respectively. However, at enough large frequencies the trend of real part can be interpreted by $Re[\sigma] = \omega^{(d-4)}$. Moreover, in holographic model the ratio ω_g/T_c is always much larger than the BCS value 3.5 due to the strong coupling of holographic superconductors. In both gravity kinds, decreasing the temperature or increasing the effect of nonlinearity shifts the gap frequency toward larger values. Besides, the gap frequency is occurred at larger values by enlarging the Gauss-Bonnet parameter. In general, the behavior of conductivity depends on the choice of the mass, the nonlinear and the Gauss-Bonnet parameters.

PACS numbers: 04.70.Bw, 11.25.Tq, 04.50.-h

I. INTRODUCTION

In recent years, the gauge/gravity duality which connects a weak gravitational system in $(d+1)$ -dimension to the strong coupling conformal field theory in d -dimension grabs a lot of attentions because it provides a powerful theoretical methods to study strong interacting systems such as high temperature superconductors [1–6]. One of the famous consequence of AdS/CFT correspondence is the appearance of a revolutionary theory which is called holographic superconductor [2]. The idea of holographic superconductor was proposed in 2008 [2] by applying AdS4/CFT3 correspondence on the probe limit in Einstein gravity. Based on this theory in order to describe a superconductor on the boundary, we need a transition from hairy black hole to a no hair black hole in the bulk for temperatures below and upper the critical value, respectively [7]. The appearance of hair corresponds to the spontaneous $U(1)$ symmetry breaking [7]. This theory opened up a new horizon in condensed matter physics to study the high temperature superconductors as well as unconventional types [2, 8]. Furthermore, holographic superconductors have widely investigated in the presence of nonlinear electrodynamics which involve more information than the usual Maxwell state. There are different kinds of nonlinear electrodynamics in the literatures such as Born-Infeld [9], Exponential [10], Logarithmic [11] and Power-Maxwell[12] electrodynamics. Many investigations have been devoted to disclose analytically as well as numerically different aspects of holographic superconductors in the presence of various kinds of (see e.g. [12–35]).

Besides the s -wave superconductors which can be described very well by the BCS theory, there are unconventional superconductors such as p -wave and d -wave superconductors[36, 37]. Unconventional superconductors can be classified as high temperature and strong coupling superconductors. It is expected that the holographic hypothesis may shed some light on this field by introducing holographic p -wave as well as d -wave superconductors. In the past decade, several researches are done to investigate the properties of unconventional superconductors based on the holographic hypothesis (see e.g. [38–51]). The holographic p -wave superconductors can be interpreted as odd parity or triplet superconductors which are constructed by coupling of electrons with parallel spins by exchange of the electronic excitations with angular momentum $\ell = 1$ [37]. The holographic p -wave superconductors have been explored from different points of view such as condensation of a complex or real charge vector field in the bulk which corresponds to the vector order parameter in the boundary or the spin-1 order parameter can be originated from the condensation

*Electronic address: mahya689mohammadi@gmail.com

†Electronic address: asheykhi@shirazu.ac.ir

of a 2-form field in the gravity side [38–42]. Introducing a $SU(2)$ Yang-Mills gauge field in the bulk in which one of the gauge degrees of freedom corresponds to the vector order parameter at the boundary, is another method to study this topic. Superconducting phase at the boundary for this type of holographic superconductors corresponds to appearance of vector hair outside the horizon by decreasing the temperature below the critical value [49].

In this work, we are going to investigate the holographic p -wave superconductors in all higher dimensions by taking into account the higher order corrections both on the gravity as well as on the gauge field sides. While, most previous works on the holographic p -wave superconductors have been investigated in the presence of the linear Maxwell field, it's interesting to examine the effects of the nonlinear electrodynamics on the properties of holographic p -wave superconductors. For the correction to the gauge field side, we consider the general nonlinear electrodynamics with higher order correction term, namely $\mathcal{L} = \mathcal{F} + b\mathcal{F}^2$. We shall do the numerical calculations for different values of the mass m and the nonlinear parameter b in each dimension to disclose the effects of these terms on the critical temperature. In all cases, we find the relation between critical temperature T_c and $\rho^{1/(d-2)}$ where ρ is regarded as charge density and plot the behavior of condensation as a function of temperature. We shall also explore the electrical conductivity by applying an appropriate perturbation on the gauge field in the background. We obtain the electrical conductivity formula and plot the behavior of the real and imaginary parts of conductivity as a function of frequency for different values of the mass and nonlinearity parameter in $d = 4, 5$ and 6 . Not only the trend of figures differs by dimension but also our choice of mass and nonlinearity has a straight effect on the behavior of conductivity. Although the obvious differences, all of them follow some universal behaviors. For example, the Kramers-Kronig relation relates the real and imaginary parts of conductivity. In low frequency regime, we observe a delta function behavior for real part while the imaginary part has a pole. The infinite DC conductivity is a feature of superconducting phase. Furthermore, we find the universality $\omega_g \simeq 8T_c$ is totally dominated but deviates in higher dimensions which is logical. Moreover, the gap frequency depends on the mass and nonlinearity parameters. Afterwards, by following the same procedure as before we do our study in Gauss-Bonnet gravity with higher order corrections in gravity and gauge fields in d -dimensional spacetime. Holographic p -wave superconductor in Gauss-Bonnet gravity previously studied in [52, 53]. We analyze the vector condensation and find that the critical temperature reduces not only by rising the mass and nonlinear parameter but also by enlarging the Gauss-Bonnet parameter α . Finally, we consider the electrical conductivity for holographic p -wave superconductor in Gauss-Bonnet gravity with higher order corrections. The global trends are also seen in this case. In this gravity, the gap frequency depends on the mass, nonlinearity and the Gauss-Bonnet parameters and the ratio of ω_g/T_c deviates from the universal value 8 by increasing the effect of α , too.

This work is outlined as follows. In section II A we introduce the holographic p -wave model in Einstein gravity through condensation a vector field. In section II B, we describe the procedure to calculate electrical conductivity based on the AdS/CFT correspondence. Section III A is devoted to conductor/superconductor phase transition in holographic setup in Gauss-Bonnet gravity. We calculate the electrical conductivity in the Gauss-Bonnet gravity with higher order corrections in section III B. Finally, we summarize our results in section IV.

II. HOLOGRAPHIC p -WAVE SUPERCONDUCTOR IN EINSTEIN GRAVITY

A. The holographic model and condensation of the vector field

We adopt the following form for the action to describe a holographic p -wave superconductor with a vector field ρ_μ with mass m and charge q

$$S = \int d^d x \sqrt{-g} [\mathcal{L}_G + \mathcal{L}_m],$$

$$\mathcal{L}_G = R - 2\Lambda, \quad \mathcal{L}_m = \mathcal{L}_{NL} - \frac{1}{2}\rho_\mu^\dagger \rho^{\mu\nu} - m^2 \rho_\mu^\dagger \rho^\mu + iq\gamma \rho_\mu \rho_\nu^\dagger F^{\mu\nu}, \quad (1)$$

where g and R are metric determinant and Ricci scalar, respectively, l is the radius of the AdS spacetime, which is related to the negative cosmological constant via

$$\Lambda = -\frac{(d-1)(d-2)}{2l^2}. \quad (2)$$

Hereafter, for simplicity we set $l = 1$. The Lagrangian density of nonlinear electrodynamics \mathcal{L}_{NL} in the Lagrangian of the matter field, \mathcal{L}_m , is given by

$$\mathcal{L}_{NL} = \mathcal{F} + b\mathcal{F}^2, \quad \mathcal{F} = -\frac{1}{4}F_{\mu\nu}F^{\mu\nu}. \quad (3)$$

When the nonlinearity parameter tends to zero, $b \rightarrow 0$, it reduces to the standard Maxwell Lagrangian, namely $\mathcal{L}_{\mathcal{NL}} \rightarrow -1/4 F_{\mu\nu} F^{\mu\nu}$ where $F_{\mu\nu} = \nabla_\mu A_\nu - \nabla_\nu A_\mu$ and $F_{\nu\mu} = \nabla_\mu A_\nu - \nabla_\nu A_\mu$. The term $b\mathcal{F}^2$ is the first order leading nonlinear correction term to the Maxwell field. There are several motivation for choosing the nonlinear Lagrangian in the form of (3). First, the series expansion of the three well-known Lagrangian of nonlinear electrodynamics such as Born-Infeld, Logarithmic and Exponential nonlinear electrodynamics have the form of (3) [54]. Second, calculating one-loop approximation of QED, it was shown [55] that the effective Lagrangian is given by (3). Besides, if one neglect all other gauge fields, one may arrive at the effective quadratic order of $U(1)$ as \mathcal{F}^2 [56, 57]. Furthermore, considering the next order correction terms in the heterotic string effective action one can obtain the \mathcal{F}^2 term as a corrections to the bosonic sector of supergravity, which has the same order as the Gauss-Bonnet term [56–58].

With the help of covariant derivative $D_\mu = \nabla_\mu - iqA_\mu$, we can define $\rho_{\mu\nu} = D_\mu \rho_\nu - D_\nu \rho_\mu$. The last term in the matter Lagrangian can be ignored in our work because it characterizes the strength of interaction between ρ_μ and A_μ with γ as the magnetic moment in the case with an applied magnetic field.

Varying action (1) with respect to the gauge field A_μ and the vector field ρ_μ , we obtain the equations of motion as

$$\nabla^\nu [(1 + 2b\mathcal{F})F_{\nu\mu}] = iq (\rho^\nu \rho^\dagger_{\nu\mu} - \rho^{\nu\dagger} \rho_{\nu\mu}) + iq\gamma \nabla^\nu (\rho_\nu \rho^\dagger_\mu - \rho^\dagger_\nu \rho_\mu), \quad (4)$$

$$D^\nu \rho_{\nu\mu} - m^2 \rho_\mu + iq\gamma \rho^\nu F_{\nu\mu} = 0. \quad (5)$$

In order to describe a d -dimensional AdS Schwarzschild black hole with flat horizon, we consider the metric as

$$ds^2 = -f(r)dt^2 + \frac{dr^2}{f(r)} + r^2 \sum_{i=1}^{d-2} dx_i^2, \quad (6)$$

$$f(r) = r^2 - \frac{r_+^{d-1}}{r^{d-3}}, \quad (7)$$

where r_+ defines the horizon location obeying $f(r_+) = 0$. While the vector and the gauge fields are assumed to have the following form

$$\rho_\nu dx^\nu = \rho_x(r)dx, \quad A_\nu dx^\nu = \phi(r)dt. \quad (8)$$

The Hawking temperature of the black hole is given by [35]

$$T = \frac{f'(r_+)}{4\pi} = \frac{(d-1)r_+}{4\pi}. \quad (9)$$

Inserting relations (6) and (8) in the field equations (4) and (5), we arrive at

$$\phi''(r) + \frac{(d-2)}{r} \left[\frac{1 + b\phi'^2(r)}{1 + 3b\phi'^2(r)} \right] \phi'(r) - \frac{2\rho_x^2(r)}{r^2 f(r) (1 + 3b\phi'^2(r))} \phi(r) = 0, \quad (10)$$

$$\rho_x''(r) + \left[\frac{(d-4)}{r} + \frac{f'(r)}{f(r)} \right] \rho_x'(r) + \left[\frac{\phi^2(r)}{f^2(r)} - \frac{m^2}{f(r)} \right] \rho_x(r) = 0. \quad (11)$$

These equations have the asymptotic solutions ($r \rightarrow \infty$) of the form

$$\rho_x(r) = \frac{\rho_{x+}}{r^{\Delta_+}} + \frac{\rho_{x-}}{r^{\Delta_-}}, \quad \phi(r) = \mu - \frac{\rho}{r^{d-3}}, \quad (12)$$

with

$$\Delta_\pm = \frac{1}{2} \left[(d-3) \pm \sqrt{(d-3)^2 + 4m^2} \right], \quad (13)$$

where our choosing masses should satisfy the Breitenlohner-Freedman (BF) bound as [59]

$$m^2 \geq -\frac{(d-3)^2}{4}. \quad (14)$$

| b=0 | | b=0.02 | | b=0.04 | |
|--------------------|--------------------|--------------------|--------------------|--------------------|--------------------|
| $m^2 = 0$ | $m^2 = 3/4$ | $m^2 = 0$ | $m^2 = 3/4$ | $m^2 = 0$ | $m^2 = 3/4$ |
| 0.125 $\rho^{1/2}$ | 0.102 $\rho^{1/2}$ | 0.120 $\rho^{1/2}$ | 0.093 $\rho^{1/2}$ | 0.115 $\rho^{1/2}$ | 0.087 $\rho^{1/2}$ |

TABLE I: Numerical results for critical temperature T_c in $d = 4$ for different values of the mass and nonlinear parameters.

| b=0 | | b=0.02 | | b=0.04 | |
|--------------------|--------------------|--------------------|--------------------|--------------------|--------------------|
| $m^2 = -3/4$ | $m^2 = 5/4$ | $m^2 = -3/4$ | $m^2 = 5/4$ | $m^2 = -3/4$ | $m^2 = 5/4$ |
| 0.224 $\rho^{1/3}$ | 0.184 $\rho^{1/3}$ | 0.212 $\rho^{1/3}$ | 0.159 $\rho^{1/3}$ | 0.204 $\rho^{1/3}$ | 0.147 $\rho^{1/3}$ |

TABLE II: Numerical results for critical temperature T_c in $d = 5$ for different values of the mass and nonlinear parameters.

Based on the AdS/CFT correspondence ρ_{x-} and ρ_{x+} are, respectively, interpreted as the source and the expectation value $\langle J_x \rangle$ which plays the role of the order parameter in the boundary theory. Moreover, μ and ρ are regarded as chemical potential and charge density in the dual field theory. In order to follow our research, we use shooting method which solves equations (10) and (11) numerically by applying suitable conditions. For this purpose, we introduce a new variable $z = r_+/r$. For convenience, we will set $r_+ = 1$ in the following calculation. We do our numerical solutions in $d = 4, 5$ and 6 and find the relation between critical temperature and $\rho^{1/(d-2)}$. We summarize our results in tables I, II and III. By analyzing the effects of mass of the vector field, we investigate the properties of the holographic superconductor for 2 values of mass in each dimension. Meanwhile, we consider the effects of nonlinearity for this model. Our results show that by increasing the value of nonlinearity parameter as well as mass makes the condensation harder to form. Figures 1-3 show the behavior of the condensation $\langle J_x \rangle^{1/(1+\Delta_+)}$ for two values of mass as a function of temperature for different values of the nonlinearity parameter in each dimension. According to these graphs, the condensation values goes up for stronger effect of the nonlinearity parameter and mass which means it is harder to have a superconductor in the presence of nonlinear electrodynamics for massive vector fields. It was already argued that holographic p -wave superconductor undergoes the first order phase transition [39, 42] in some cases instead of usual second order type. However, in our work with these choices for the mass and nonlinear parameters, we don't observe this phenomenon. It may occur in the presence of backreaction parameter or for other values of the mass and nonlinear parameters.

B. Electrical conductivity

In this section, we are going to calculate the electrical conductivity as a function of frequency for this holographic superconductor in the presence of nonlinear electrodynamics. To follow our aim, we apply appropriate electromagnetic perturbation as $\delta A_y = A_y e^{-i\omega t}$ on the black hole background which based on the AdS/CFT duality corresponds to the boundary electrical current. We choose this form of perturbation for simplicity same as [42, 52, 53]. The consequence of turning on this perturbation in gauge field occurs in y -component of equation (4) as

$$A_y''(r) + \left[\frac{(d-4)}{r} + \frac{f'(r)}{f(r)} + \frac{2b\phi'(r)\phi''(r)}{1+b\phi'^2(r)} \right] A_y'(r) + \left[\frac{\omega^2}{f^2(r)} - \frac{2\rho_x^2(r)}{r^2 f(r) (1+b\phi'^2(r))} \right] A_y(r) = 0, \quad (15)$$

which has the asymptotic behavior as

$$A_y''(r) + \frac{(d-2)}{r} A_y'(r) + \frac{\omega^2}{r^4} A_y(r) = 0, \quad (16)$$

by considering $A^{(0)}$ and $A^{(1)}$ as constant parameters, we have the following solution for A_y asymptotically

$$A_y = \begin{cases} A^{(0)} + \frac{A^{(1)}}{r} + \dots, & d = 4 \\ A^{(0)} + \frac{A^{(1)}}{r^2} + \frac{A^{(0)}\omega^2 \log(\Lambda r)}{2r^2} + \dots, & d = 5 \\ A^{(0)} + \frac{A^{(1)}}{r^3} + \frac{A^{(0)}\omega^2}{2r^2} + \dots, & d = 6 \end{cases} \quad (17)$$

| b=0 | | b=0.02 | | b=0.04 | |
|--------------------|--------------------|--------------------|--------------------|--------------------|--------------------|
| $m^2 = -5/4$ | $m^2 = -2$ | $m^2 = -5/4$ | $m^2 = -2$ | $m^2 = -5/4$ | $m^2 = -2$ |
| 0.289 $\rho^{1/4}$ | 0.312 $\rho^{1/4}$ | 0.261 $\rho^{1/4}$ | 0.292 $\rho^{1/4}$ | 0.247 $\rho^{1/4}$ | 0.281 $\rho^{1/4}$ |

TABLE III: Numerical results for critical temperature T_c in $d = 6$ for different values of mass and nonlinearity parameters.

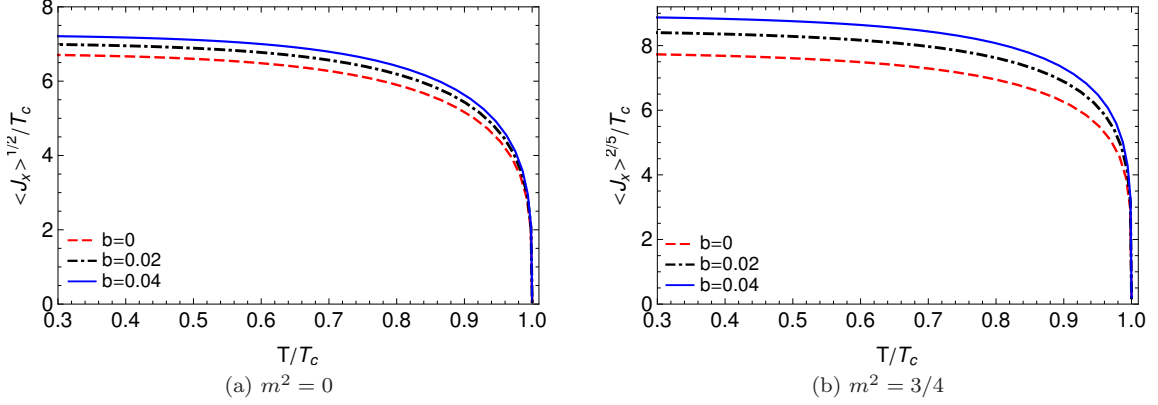


FIG. 1: The behavior of the condensation parameter as a function of the temperature for different values of the mass and nonlinearity parameters in $d = 4$.

where Λ is an arbitrary constant. Equations (16) and (17) are the same as corresponding equations in s -wave case[26]. According to the AdS/CFT correspondence, the electrical current based on on-shell bulk action $S_{o.s}$ and the Lagrangian of the matter field \mathcal{L}_m is defined by

$$J = \frac{\delta S_{\text{bulk}}}{\delta A^{(0)}} = \frac{\delta S_{o.s}}{\delta A^{(0)}} = \frac{\partial(\sqrt{-g}\mathcal{L}_m)}{\partial A'_y}|_{r \rightarrow \infty}, \quad (18)$$

where

$$S_{o.s.} = \int_{r_+}^{\infty} dr \int d^{d-1}x \sqrt{-g} \mathcal{L}_m, \quad (19)$$

by inserting (17) in (19), we arrive at

$$S_{o.s.} = -\frac{1}{2} \int d^{d-1}x [A_y(r)f(r)A'_y(r)(1 + b\phi'^2(r))] r^{d-4}. \quad (20)$$

Pursuing the AdS/CFT framework, the electrical conductivity is

$$\sigma_{yy} = \frac{J_y}{E_y}, \quad E_y = -\partial_t \delta A_y. \quad (21)$$

Therefore, the electrical conductivity, based on holographic approach by using Eqs. (18), (19) and (21) and adding appropriate counterterms for $d = 5$ and 6 to remove the divergency based on the re-normalization method [60] is

$$\sigma_{yy} = \begin{cases} \frac{A^{(1)}}{i\omega A^{(0)}}, & d = 4 \\ \frac{2A^{(1)}}{i\omega A^{(0)}} + \frac{i\omega}{2}, & d = 5 \\ \frac{3A^{(1)}}{i\omega A^{(0)}}, & d = 6 \end{cases} \quad (22)$$

which is in complete agreement with the σ_{xx} obtained in [26]. This shows that the calculation of σ_{yy} in holographic p -wave superconductor is the same as σ_{xx} in holographic s -wave superconductor[52]. In order to investigate the trend

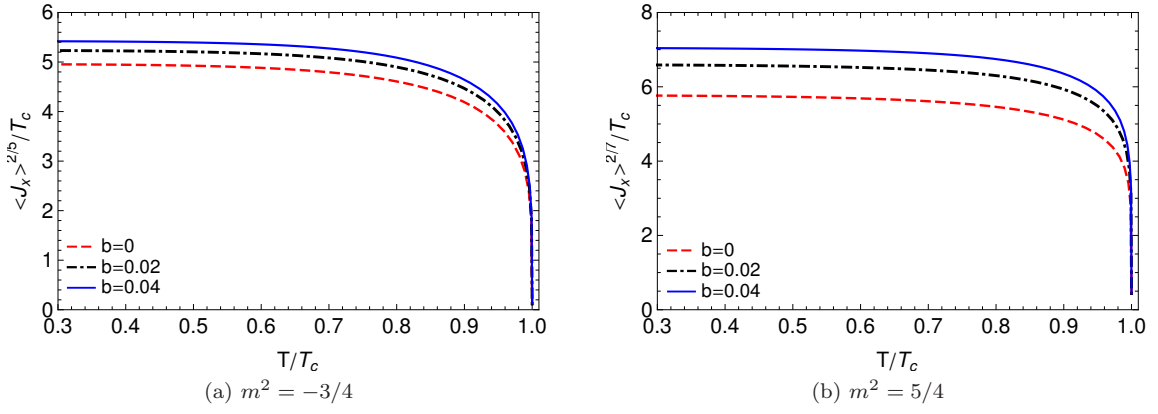


FIG. 2: The behavior of the condensation parameter as a function of the temperature for different values of mass and nonlinearity parameters in $d = 5$.

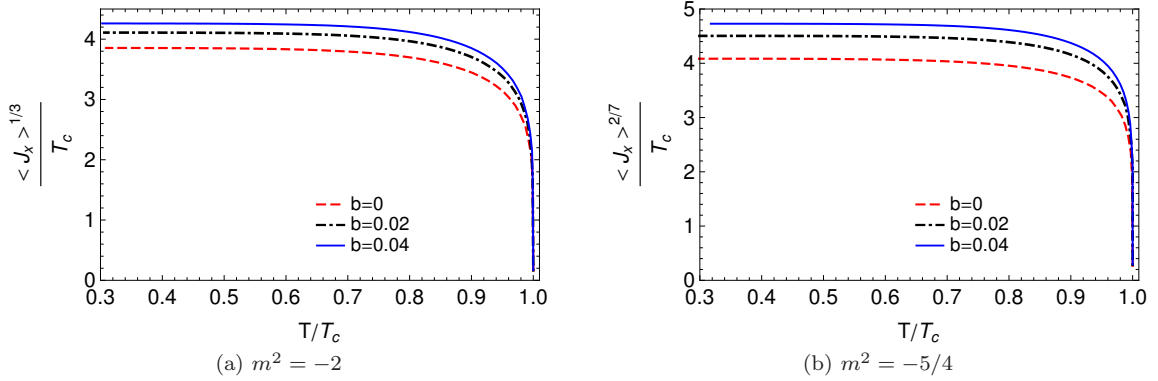


FIG. 3: The behavior of the condensation parameter as a function of the temperature for different values of mass and nonlinearity parameters in $d = 6$.

of conductivity numerically, we impose the ingoing wave boundary condition near the horizon for A_y as follows

$$A_y(r) = f(r)^{-i\omega/(4\pi T)} [1 + a(1-r) + b(1-r) + \dots], \quad (23)$$

where the Hawking temperature is expressed by T and a, b, \dots are coefficients which can be obtained by Taylor expansion of Eq. (16) around the horizon. Figs. 4-9 illustrate the behavior of real and imaginary parts of conductivity as a function of ω/T for different values of mass and nonlinearity parameters in different dimensions. In spite of the fact that there are obvious differences in figures, they follow some universal behaviors. First of all, the real part of conductivity is related to the imaginary side based on the Kramers-Kronig relation which means that the appearance of the delta function and pole in real and imaginary parts of conductivity, respectively. Secondly, the superconducting gap which appears below the critical temperature becomes deeper and sharper by diminishing the temperature which causes larger values of ω_g . This fact approved the results of previous section about condensation by going down the temperature because we can interpret ω_g as the energy to break the fermion pairs. So, the bigger values of ω_g leads to harder formation of fermion pairs which hinders the conductor/superconductor phase transition [52]. At large frequencies, the behavior of conductivity can be indicated to have a power law behavior as $Re[\sigma] = \omega^{(d-4)}$ similar to s -wave case [26]. In addition, based on the BCS theory $\omega_g \approx 3.5T_c$ while in holographic setup the ratio of gap frequency over critical temperature is found to be the universal value around 8 which hints to the fact that in BCS theory the pairs couple to each other weakly with no interaction. However, the holographic superconductors are strongly coupled. This strong coupling is the reason that we use holographic model to describe high temperature superconductors which exist in strong coupling regime [52]. Due to describe details more, we should say that the peak of real part of conductivity follows the same trend as the minimum value of imaginary part by decreasing the temperature. They shift toward the larger frequencies in all dimensions. Our choice of the mass has a direct outcome on the behavior of conductivity that becomes so obvious in some cases. For example, in $d = 5$ we face with sharp peak and deep minimum in real and imaginary parts for $m^2 = -3/4$ while for the case that the vector field has a

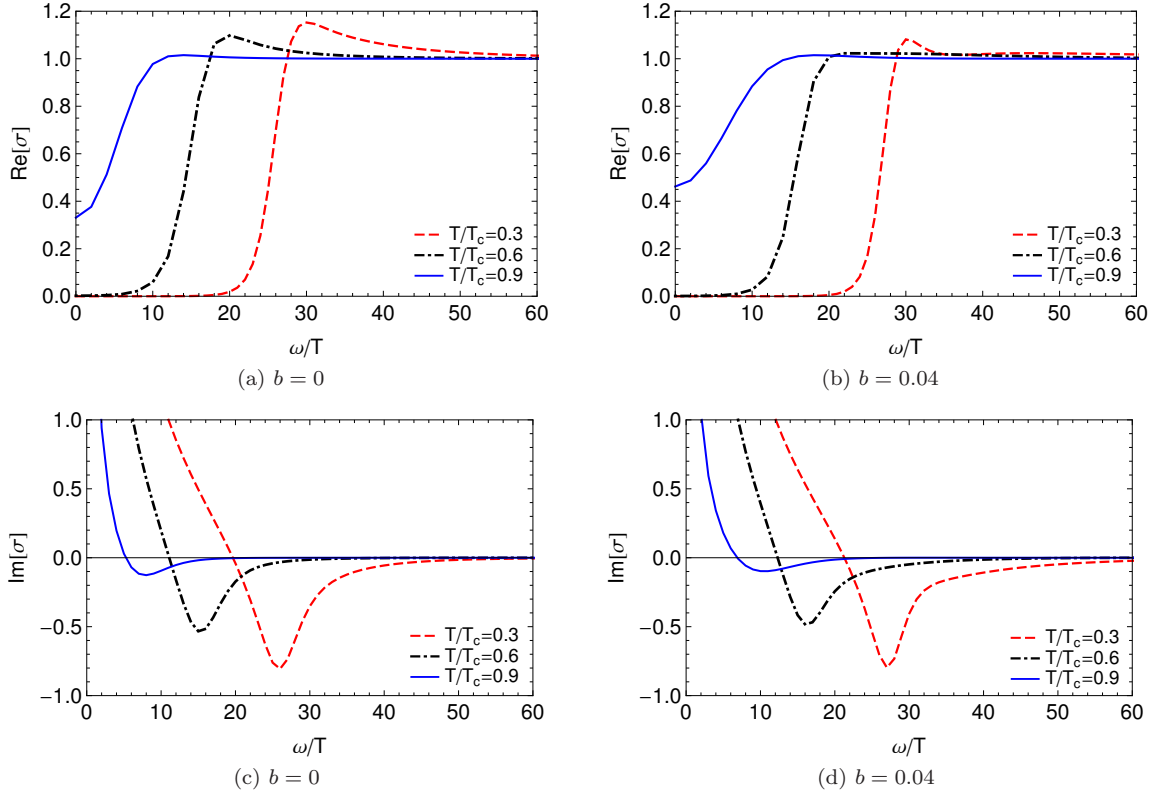


FIG. 4: The behavior of real and imaginary parts of conductivity for $m^2 = 0$ in $d = 4$.

mass equals to $m^2 = 5/4$ we observe smooth peak and minimum in two parts of conductivity. Overall, it seems that $T = 0.3T_c$ has a strong effect on conductivity in $d = 5$ and 6 . In order to study the effect of nonlinear electrodynamics on the conductivity, we plot its behavior in fixed temperature $T = 0.3T_c$ in figs. 10-11. According to this graphs, the effects of nonlinearity parameter on conductivity is straightly depend on the mass and dimension. For example, in $d = 4$ and for $d = 5$ with $m^2 = 5/4$ increasing the nonlinearity makes the peak and minimum parts more smooth and flat. However, for other cases doesn't behave like that. In $d = 6$, increasing the nonlinearity causes smaller first gap and enlarging the second one in real part of conductivity. In general, the gap frequency is shifted in the presence of nonlinear electrodynamics.

III. HOLOGRAPHIC p -WAVE SUPERCONDUCTOR IN GAUSS-BONNET GRAVITY

A. Conductor/superconductor phase transition in holographic setup

In this section, we want to study the condensation of the vector field in the background of the AdS black holes with higher order corrections both in the gravity and gauge field. We write down the action in the following form

$$\begin{aligned}
 S &= \int d^d x \sqrt{-g} [\mathcal{L}_G + \mathcal{L}_m], \\
 \mathcal{L}_G &= R - 2\Lambda + \frac{\alpha}{2} [R^2 - 4R^{\mu\nu} R_{\mu\nu} + R^{\mu\nu\rho\sigma} R_{\mu\nu\rho\sigma}], \\
 \mathcal{L}_m &= \mathcal{L}_{NL} - \frac{1}{2} \rho_{\mu\nu}^\dagger \rho^{\mu\nu} - m^2 \rho_\mu^\dagger \rho^\mu + i q \gamma \rho_\mu \rho_\nu^\dagger F^{\mu\nu},
 \end{aligned} \tag{24}$$

where for same parameters as section II A, we have similar definition while the Gauss-Bonnet parameter, Ricci tensor and Riemann curvature tensor are defined, respectively, by α , $R_{\mu\nu}$ and $R_{\mu\nu\rho\sigma}$. When $\alpha \rightarrow 0$, the above action reduces

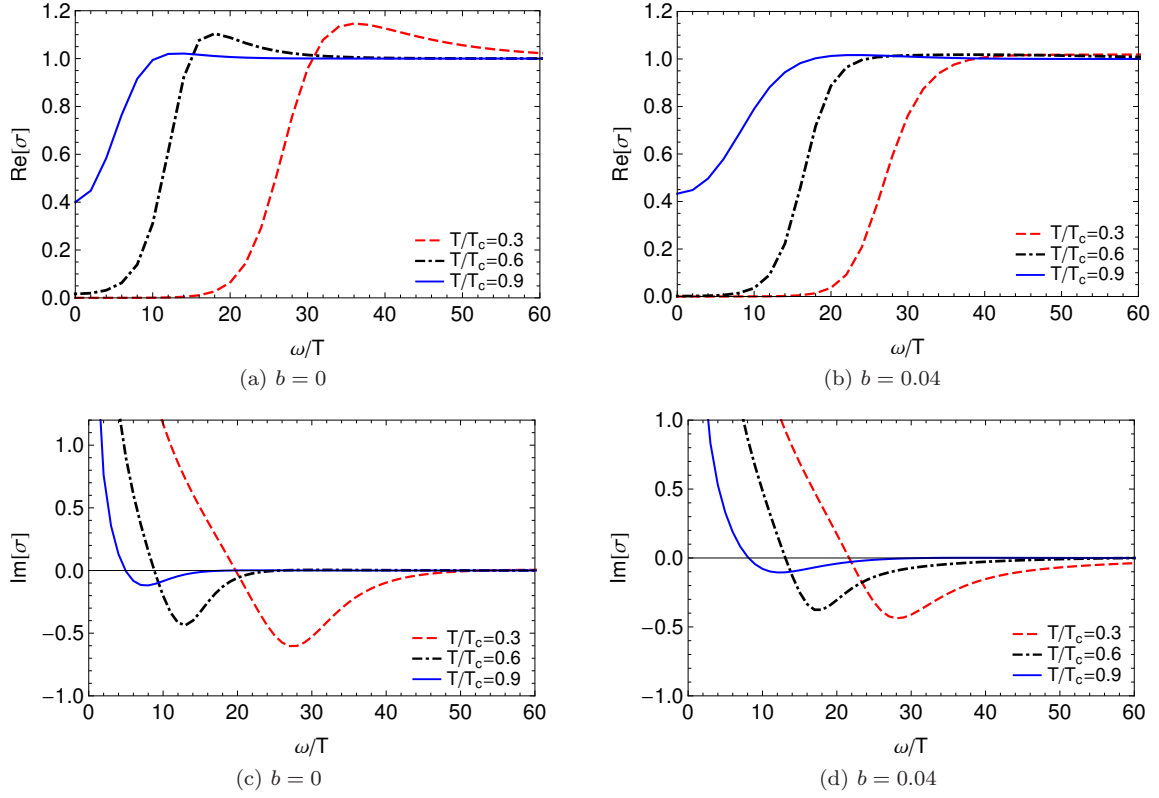


FIG. 5: The behavior of real and imaginary parts of conductivity for $m^2 = 3/4$ in $d = 4$.

to Einstein one. We take the line elements of the spacetime metric as

$$ds^2 = -f(r)dt^2 + \frac{dr^2}{f(r)} + r^2 \sum_{i=1}^{d-2} dx_i^2, \quad (25)$$

$$f(r) = \frac{r^2}{2\alpha} \left[1 - \sqrt{1 - 4\alpha \left(1 - \frac{1}{r^{d-1}} \right)} \right], \quad (26)$$

where the function $f(r)$ has the asymptotic behavior as

$$f(r) = \frac{r^2}{2\alpha} [1 - \sqrt{1 - 4\alpha}]. \quad (27)$$

We can present the effective radius L_{eff} for the AdS spacetime as [52]

$$L_{\text{eff}}^2 = \frac{2\alpha}{1 - \sqrt{1 - 4\alpha}}. \quad (28)$$

Based on the above equation, in order to have a well-defined vacuum expectation value $\alpha \leq 1/4$ where the upper bound $\alpha = 1/4$ is called Chern-Simon limit [52]. Besides, in the CFT side we consider the causality constraint on our choice of Gauss-Bonnet parameter with $-7/36 \leq \alpha \leq 9/100$ and $-51/196 \leq \alpha \leq 32/256$ for AdS5/CFT4 and AdS6/CFT5, respectively[61–67]. We choose the vector and gauge fields same as equation (8). By variation the equation (24) with respect to gauge and vector fields, same equations as equations (4) and (5) were obtained. Moreover, the equations (10) and (11) with the asymptotic behavior as (12) are recovered, finally. Equation (13) in Gauss-Bonnet gravity changes to

$$\Delta_{\pm} = \frac{1}{2} \left[(d-3) \pm \sqrt{(d-3)^2 + 4m^2 L_{\text{eff}}^2} \right], \quad (29)$$

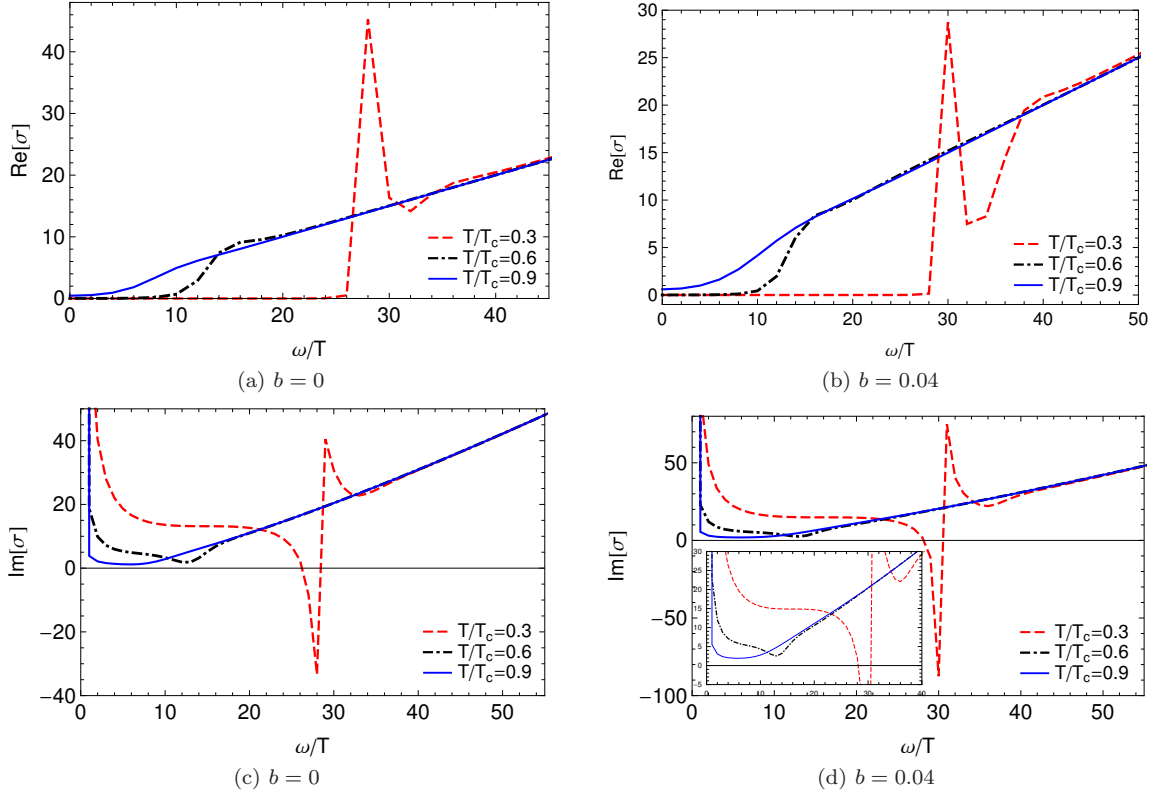


FIG. 6: The behavior of real and imaginary parts of conductivity for $m^2 = -3/4$ in $d = 5$.

with the Breitenlohner-Freedman (BF) bound as

$$\bar{m}^2 \geq -\frac{(d-3)^2}{4}, \quad \bar{m}^2 = m^2 L_{\text{eff}}^2. \quad (30)$$

In the Maxwell limit where $b \rightarrow 0$, field equations turn to corresponding equations in equation [52]. In addition, the Hawking temperature equals to equation (9). The numerical results are listed in tables IV and V. In order to compare our results with [52] and [53], we choose $\Delta_+ = 3/2$ and 2 in $d = 5$ dimension. There is a perfect agreement between our results with corresponding cases in [52] and [53]. However, because of the difficulty of numerical solution, we can only do our study for one value of mass in $d = 6$. Tables IV and V give information about the values of critical temperature T_c based on $\rho^{1/(d-2)}$ for different effects of the mass and nonlinear parameters as well as Gauss-Bonnet parameter. Increasing the Gauss-Bonnet coefficient has the same effect as larger values of mass and nonlinear parameters on the critical temperatures. We also face with diminishing of critical temperature for stronger values of α which makes the condensation harder to form by putting off the appearance of hair in gravity side which corresponds to superconducting phase in boundary field theory. Moreover, the results in $d = 5$ with $\bar{m}^2 = -3/4$ and $\alpha = 0.0001$ are alike the outcomes of corresponding case in Einstein gravity. This is rooted in the fact that as said before in $\alpha \rightarrow 0$ limit, the Einstein case is regained. Meanwhile, figs. 12-17 show the behavior of condensation as a function of temperature in different choices of mass, nonlinearity and Gauss-Bonnet parameters. Increasing each one of these three parameters makes the condensation value raising. Furthermore, the effect of different values of Gauss-Bonnet parameter becomes more and more obvious by growing the nonlinear parameter b . Based on the obtained results and same as [52] the Gauss-Bonnet term doesn't change the critical exponent of condensation which means that we face with second order phase transition for all values of α , the same as section II A.

B. Conductivity

In order to study the electrical conductivity for holographic p -wave superconductor in the Gauss-Bonnet gravity, we follow the same approach as section II B. By choosing the same perturbation as $\delta A_y = A_y e^{-i\omega t}$, we obtain the

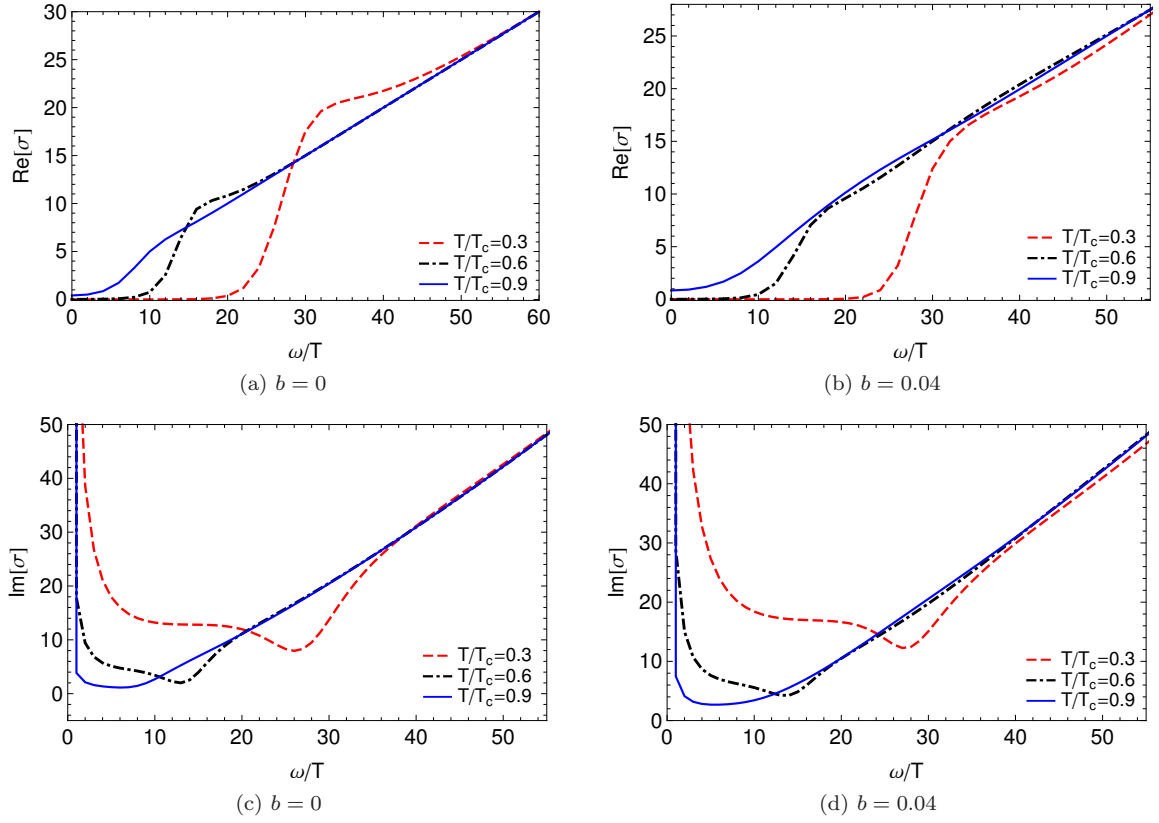


FIG. 7: The behavior of real and imaginary parts of conductivity for $m^2 = 5/4$ in $d = 5$.

| | $b = 0$ | | $b = 0.02$ | | $b = 0.04$ | |
|-------------------|-------------------------|----------------------|-------------------------|----------------------|-------------------------|----------------------|
| | $\overline{m}^2 = -3/4$ | $\overline{m}^2 = 0$ | $\overline{m}^2 = -3/4$ | $\overline{m}^2 = 0$ | $\overline{m}^2 = -3/4$ | $\overline{m}^2 = 0$ |
| $\alpha = 0.08$ | $0.218 \rho^{1/3}$ | $0.195 \rho^{1/3}$ | $0.204 \rho^{1/3}$ | $0.174 \rho^{1/3}$ | $0.196 \rho^{1/3}$ | $0.163 \rho^{1/3}$ |
| $\alpha = 0.0001$ | $0.224 \rho^{1/3}$ | $0.200 \rho^{1/3}$ | $0.218 \rho^{1/3}$ | $0.181 \rho^{1/3}$ | $0.204 \rho^{1/3}$ | $0.171 \rho^{1/3}$ |
| $\alpha = -0.08$ | $0.229 \rho^{1/3}$ | $0.205 \rho^{1/3}$ | $0.218 \rho^{1/3}$ | $0.187 \rho^{1/3}$ | $0.210 \rho^{1/3}$ | $0.177 \rho^{1/3}$ |

TABLE IV: Numerical results for critical temperature T_c in $d = 5$ for different values of mass, nonlinearity and Gauss-Bonnet parameters.

linearized equation as (15) with the asymptotic behavior ($r \rightarrow \infty$) as

$$A_y''(r) + \frac{(d-2)}{r} A_y'(r) + \frac{\omega^2 L_{\text{eff}}^4}{r^4} A_y(r) = 0, \quad (31)$$

which has the solution as follows

$$A_y = \begin{cases} A^{(0)} + \frac{A^{(1)}}{r^2} + \frac{A^{(0)} \omega^2 L_{\text{eff}}^4 \log(\Lambda r)}{2r^2} + \dots, & d = 5 \\ A^{(0)} + \frac{A^{(1)}}{r^3} + \frac{A^{(0)} \omega^2 L_{\text{eff}}^4}{2r^2} + \dots, & d = 6 \end{cases} \quad (32)$$

which is similar to equation (17) except the L_{eff}^4 term which shows the influence of Gauss-Bonnet gravity. By pursuing the identical procedure as section II B, equations (18), (19), (20) and (21) are regained. So, the electrical conductivity

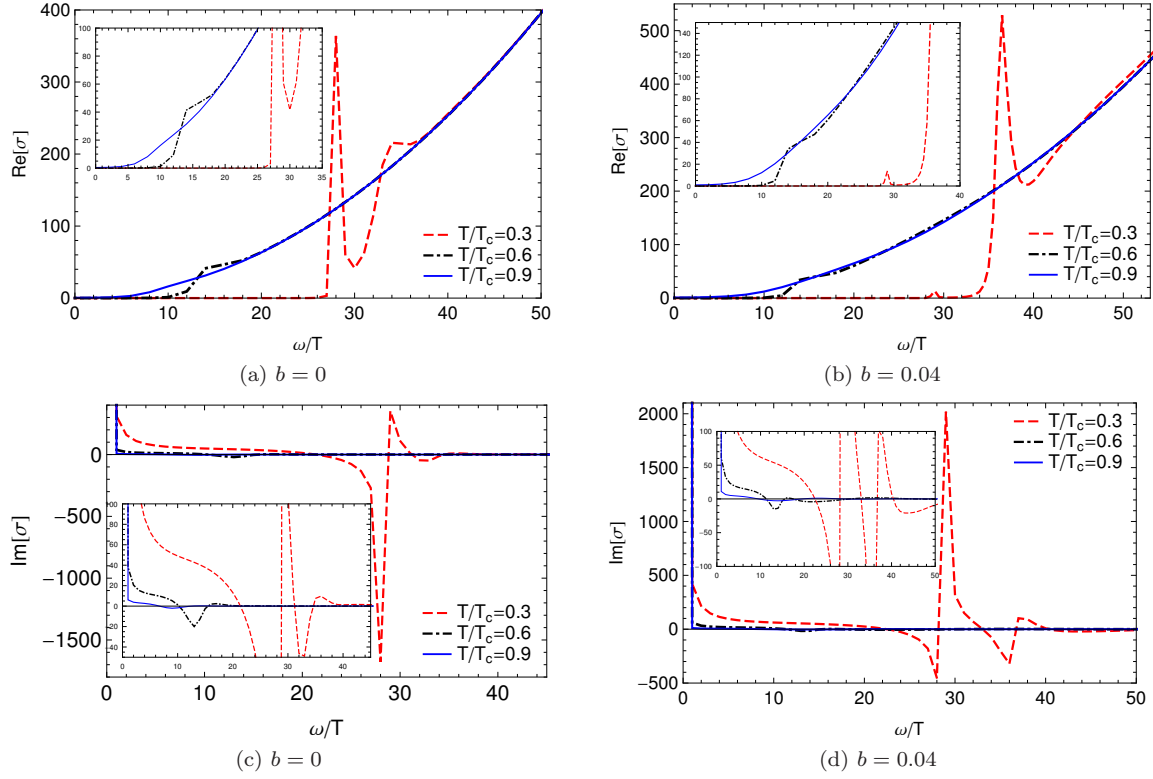


FIG. 8: The behavior of real and imaginary parts of conductivity for $m^2 = -5/4$ in $d = 6$.

| | $b = 0$ | $b = 0.02$ | $b = 0.04$ |
|-------------------|--------------------|--------------------|--------------------|
| $\alpha = 0.08$ | $0.267 \rho^{1/4}$ | $0.228 \rho^{1/4}$ | $0.212 \rho^{1/4}$ |
| $\alpha = 0.0001$ | $0.273 \rho^{1/4}$ | $0.236 \rho^{1/4}$ | $0.221 \rho^{1/4}$ |
| $\alpha = -0.08$ | $0.277 \rho^{1/4}$ | $0.243 \rho^{1/4}$ | $0.228 \rho^{1/4}$ |

TABLE V: Numerical results for critical temperature T_c with $\overline{m}^2 = 0$ in $d = 6$ for different values of nonlinearity and Gauss-Bonnet parameters.

based on holographic approach in Gauss-Bonnet gravity can be expressed by

$$\sigma_{yy} = \begin{cases} \frac{2A^{(1)}}{i\omega L_{\text{eff}}^2 A^{(0)}} + \frac{i\omega L_{\text{eff}}^2}{2}, & d = 5 \\ \frac{3A^{(1)}}{i\omega L_{\text{eff}}^2 A^{(0)}}, & d = 6 \end{cases} \quad (33)$$

Again like section II B, definition of σ_{yy} is same as σ_{xx} in Ref. [27] which confirms the fact that calculation of σ_{yy} in holographic p -wave superconductors is similar to σ_{xx} in holographic s -wave superconductors. Next, by expanding A_y as equation (23) we can plot the behavior of real and imaginary parts of conductivity as a function of frequency for different values of the nonlinearity, mass and Gauss-Bonnet parameters in $d = 5$ and 6 in figs. 18-23. Although the differences in figures, they show the universality trend same as conductivity behavior in the Einstein gravity which explained in section II B. In $\omega \rightarrow 0$ limit, the delta function behavior of real part of conductivity is related to imaginary part which has a pole in this region through Kramers-Kronig relation. The infinite DC conductivity is a tail of superconducting phase. On the other hand, at large frequency regime the behavior of real part of conductivity can be expressed by $Re[\sigma] = \omega^{(d-4)}$. Furthermore, for holographic p -wave superconductor in Gauss-Bonnet gravity $\omega_g \approx 8T_c$ which is much more than the BSC value (3.5). This difference is originated from the fact that the strong interaction governs in holographic superconductors similar to [52]. However, we observe the deviation from 8 by increasing the nonlinearity as well as Gauss-Bonnet parameters. Increasing the nonlinearity and Gauss-Bonnet parameters or decreasing the temperature while the other two components are fixed, shifts the maximum and minimum values of real

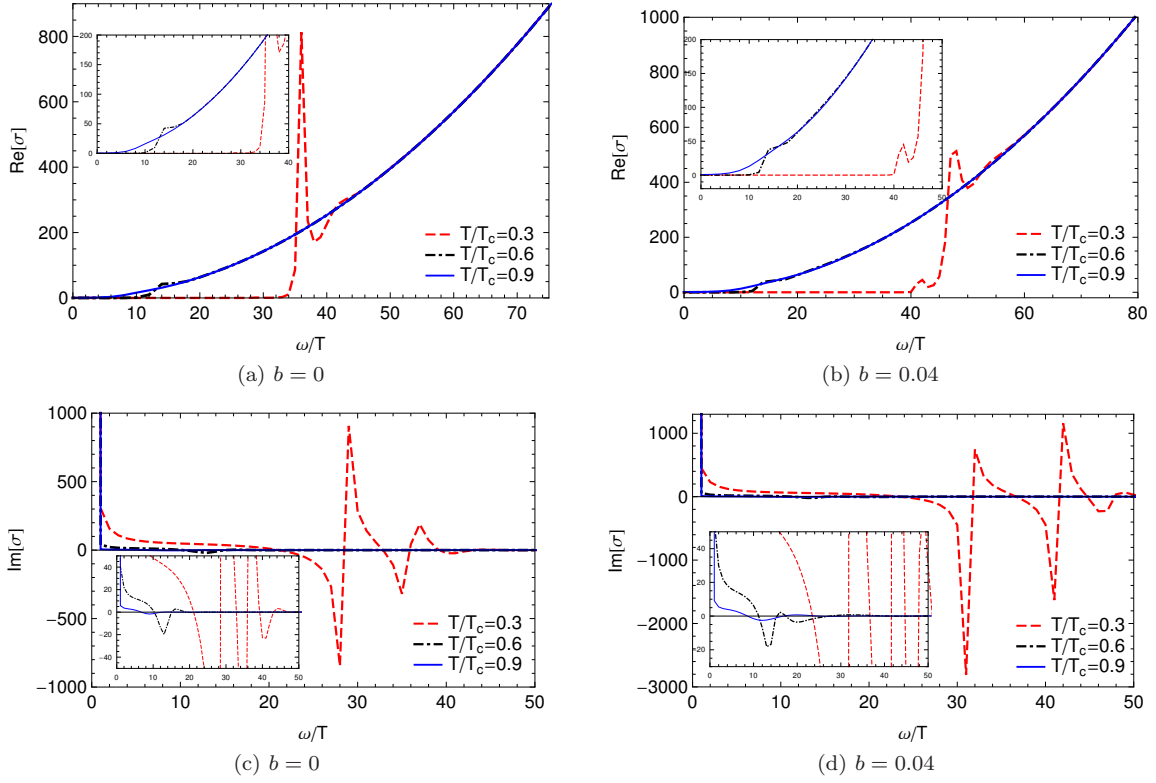


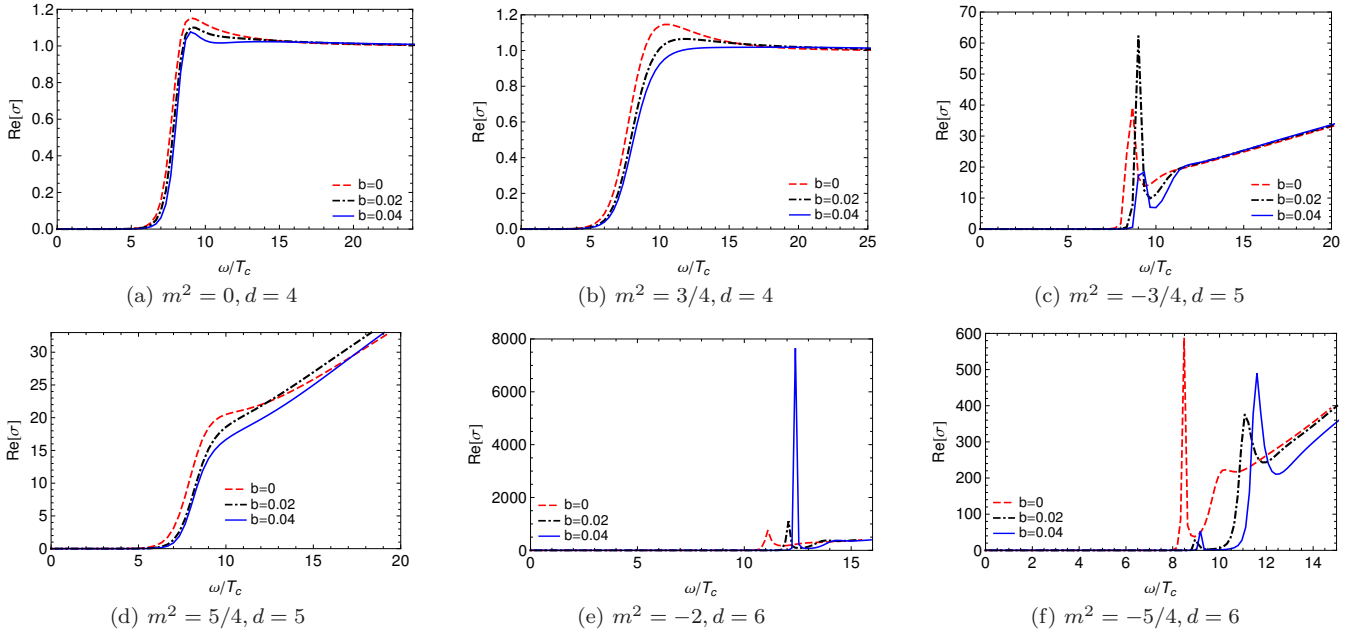
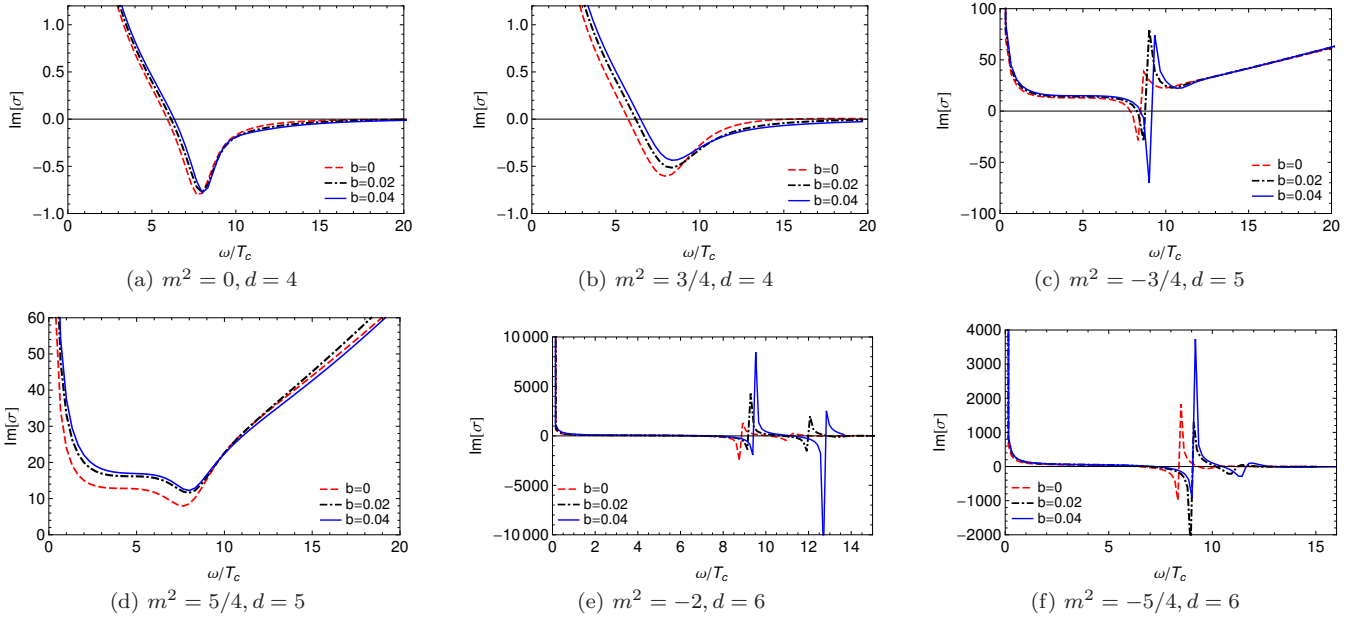
FIG. 9: The behavior of real and imaginary parts of conductivity for $m^2 = -2$ in $d = 6$.

and imaginary parts toward larger frequencies. Based on [52] for the fixed values of temperature, real and imaginary parts of conductivity diminish by enlarging the Gauss-Bonnet effect. It's true in some cases in the presence of Maxwell electrodynamics. For example, the behavior of real parts of conductivity in $d = 5$ with $\bar{m}^2 = -3/4$ confirms this idea while in the same dimension with $\bar{m}^2 = 0$, it doesn't follow the same trend. However, this idea doesn't govern more in nonlinear regime. In general, we can say that the gap frequency depends on mass, nonlinearity and Gauss-Bonnet parameters in each dimension. The dependence of conductivity to nonlinearity and Gauss-Bonnet parameters are shown in figs. 24-27.

IV. SUMMARY AND CONCLUSION

In this work, by applying AdS/CFT correspondence in higher dimensional spacetime, we have analyzed the behavior of holographic p -wave superconductor by considering the higher order corrections in gravity as well as gauge field side. First of all, we studied the condensation of vector field in the presence of nonlinear correction to the electrodynamics as given in Eq. (3). This equation can be considered as the leading order expansion terms of the well-known Born-Infeld, Logarithmic and Exponential nonlinear electrodynamics. After finding equations of motion in Einstein gravity, we solved them numerically by applying suitable conditions and investigated the effect of mass, dimension and nonlinear parameters. We found out the relation between critical temperature T_c and $\rho^{1/(d-2)}$ in all cases. Then, we plotted the behavior of condensation as a function of temperature. Based on the obtained results, we found out that increasing the value of the mass as well as nonlinearity decreases the critical temperature. This makes the condensation harder to form. Also by taking look at graphs, we understand that the condensation value enlarges for stronger effect of the mass and nonlinearity which means that vector hair faces with difficulty to occur. It was argued in [39, 42] that the holographic p -wave superconductors undergo first order phase transition instead of usual second type in some situations but we didn't observe such a behavior.

Next, in section II B we have numerically investigated the behavior of electrical conductivity as a function of frequency. For this purpose, we applied an electromagnetic perturbation as $\delta A_y = A_y e^{-i\omega t}$ in gravity side which corresponds to electrical current in CFT part. We presented the electrical conductivity formula in $d = 4, 5$ and 6 and graphs of real and imaginary parts. The conductivity differs based on our choice of mass, dimension and nonlinearity. However, some global trends were observed. Firstly, the real and imaginary parts follow the Kramers-Kronig relation

FIG. 10: The behavior of real parts of conductivity for $T/T_c = 0.3$.FIG. 11: The behavior of imaginary parts of conductivity for $T/T_c = 0.3$.

by having a delta function and divergence behavior in the low frequency regime. Infinite DC conductivity is a feature of superconducting phase. Secondly, at large enough frequencies, the behavior of the real part can be interpreted by $Re[\sigma] = \omega^{(d-4)}$. Thirdly, the ratio of ω_g/T_c in all cases is much larger than the BCS value (3.5) because holographic superconductors are strongly coupled. In holographic setup in many cases we found $\omega_g \simeq 8T_c$ while a deviation from this value occurred by increasing the dimension and nonlinearity effect. The presence of nonlinear electrodynamics shifts the gap frequency toward larger values. In section III A, with the same procedure as section II A, we found the ratio of $T_c/\rho^{1/(d-2)}$ numerically and achieved the trend of condensation versus temperature for different values of mass, nonlinearity and Gauss-Bonnet parameters in different dimensions for holographic p -wave superconductor in Gauss-Bonnet gravity. Increasing the effect of mass and nonlinear parameter follows the same behavior as Einstein case. Furthermore, going up the Gauss-Bonnet parameter α hinders the superconducting phase by diminishing the

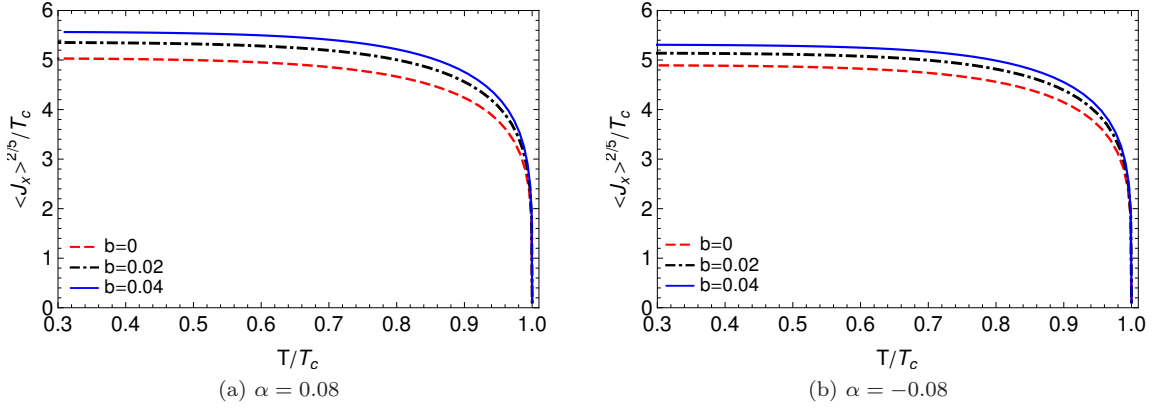


FIG. 12: The behavior of the condensation parameter as a function of the temperature for different values of nonlinearity parameters in $d = 5$ with $\overline{m}^2 = -3/4$.

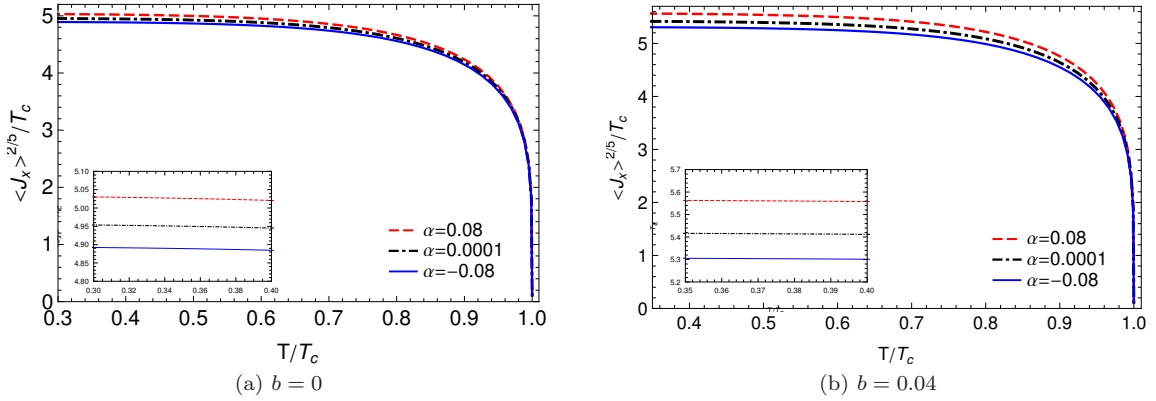


FIG. 13: The behavior of the condensation parameter as a function of the temperature for different values of Gauss-Bonnet parameters in $d = 5$ with $\overline{m}^2 = -3/4$.

critical temperature. Besides, the Gauss-Bonnet term α doesn't change the order of phase transition. In section III B, the electrical conductivity of $(d + 1)$ -dimensional holographic p -wave superconductor in Gauss-Bonnet gravity with higher order corrections in gravity and gauge fields was studied. Same as section II B, the conductivity formula and behavior of real and imaginary parts impressed by mass, nonlinearity and Gauss-Bonnet parameters in different dimensions were obtained. The universal behaviors same as Einstein case were achieved. In addition, increasing the effect of nonlinear and Gauss-Bonnet parameters or decreasing the temperature shifts the gap energy toward larger frequencies. In general, the gap frequency ω_g is depended on mass, nonlinearity and Gauss-Bonnet terms. It would be interesting to investigate the effect of backreaction in this case.

Acknowledgments

We thank Shiraz University Research Council. The work of AS has been supported financially by Research Institute for Astronomy and Astrophysics of Maragha (RIAAM), Iran.

-
- [1] J. M. Maldacena, Adv. Theor. Math. Phys. **2**, 231 (1998) [arXiv:hep-th/9711200v3].
 - [2] S. A. Hartnoll, C. P. Herzog and G. T. Horowitz, Phys. Rev. Lett. **101**, 031601 (2008) [arXiv:0803.3295].
 - [3] S. S. Gubser, I. R. Klebanov and A. M. Polyakov, Phys. Lett. B **428**, 105 (1998) [arXiv:hep-th/9802109].
 - [4] E. Witten, Adv. Theor. Math. Phys. **2**, 253 (1998) [arXiv:hep-th/9802150].
 - [5] G. T. Horowitz and M. M. Roberts, Phys. Rev. D **78**, 126008 (2008).

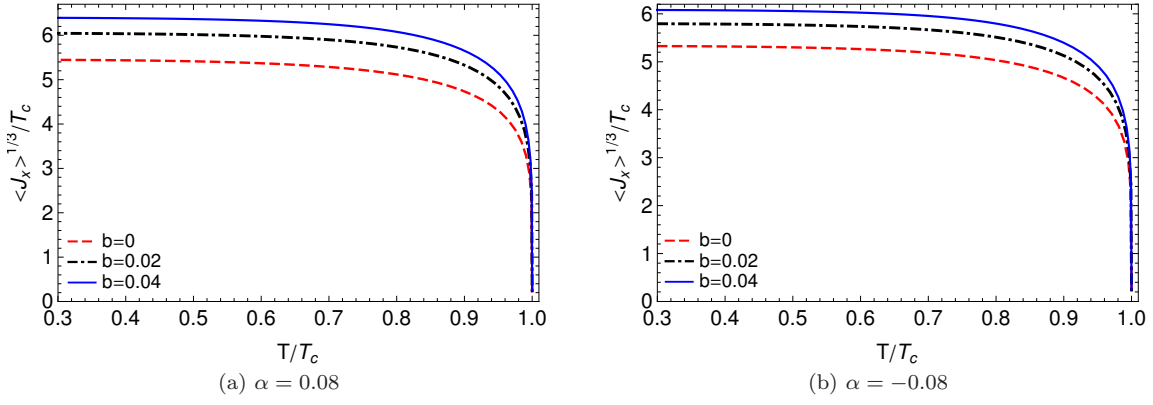


FIG. 14: The behavior of the condensation parameter as a function of the temperature for different values of nonlinearity parameters in $d = 5$ with $\overline{m}^2 = 0$.

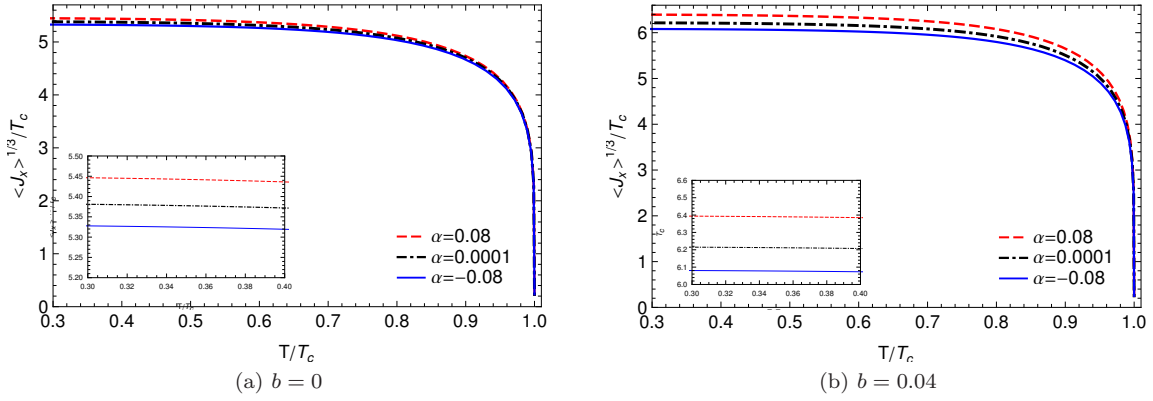


FIG. 15: The behavior of the condensation parameter as a function of the temperature for different values of Gauss-Bonnet parameters in $d = 5$ with $\overline{m}^2 = 0$.

- [6] J. Ren, JHEP. **1011**, 055 (2010) [arXiv:1008.3904].
- [7] G. T. Horowitz, Lect. Notes Phys. **828**, 313 (2011) [arXiv:1002.1722].
- [8] S. A. Hartnoll, Class. Quantum Grav. **26**, 224002 (2009) [arXiv:0903.3246].
- [9] M. Born and L. Infeld, Proc. R. Soc. A **144**, 425 (1934).
- [10] S.H. Hendi and A. Sheykhi, Phys. Rev. D, **88**, 044044 . [arXiv:1405.6998].
- [11] H. H. Soleng, Phys. Rev. D **52**, 6178 (1995), [arXiv:hep-th/9509033].
- [12] H. R. Salahi, A. Sheykhi, A. Montakhab, Eur. Phys. J. C **76**, 575 (2016) [arXiv:1608.05025].
- [13] C. P. Herzog, J. Phys. A **42**, 343001 (2009) [arXiv:0904.1975].
- [14] S. S. Gubser, C. P. Herzog, S. S. Pufu and T. Tesileanu, Phys. Rev. Lett. **103**, 141601 (2009) [arXiv:0907.3510].
- [15] S. A. Hartnoll, C. P. Herzog and G. T. Horowitz, JHEP **0812**, 015 (2008) [arXiv:0810.1563].
- [16] J. Jing, S. Chen, Phys. Lett. B **686**, 68 (2010) [arXiv:1001.4227].
- [17] R. G. Cai, L. Li, Li-Fang Li, Run-Qiu Yang, Sci China Phys. Mech. Astron. **58**, 060401 (2015) [arXiv:1502.00437].
- [18] X. H. Ge, B. Wang, S. F. Wu, and G. H. Yang, JHEP **1008**, 108 (2010) [arXiv:1002.4901].
- [19] X. H. Ge, S. F. Tu, B. Wang, JHEP **09**, 088 (2012) [arXiv:1209.4272].
- [20] X. M. Kuang, E. Papantonopoulos, G. Siopsis, B. Wang, Phys. Rev. D **88**, 086008 (2013) [arXiv:1303.2575].
- [21] Q. Pan, J. Jing, B. Wang, JHEP **11**, 088 (2011) [arXiv:1105.6153].
- [22] R. G. Cai, H. F. Li, H.Q. Zhang, Phys. Rev. D **83**, 126007 (2011).
- [23] R. G. Cai, Z.Y. Nie, H.Q. Zhang, Phys. Rev. D **82**, 066007 (2010).
- [24] W. Yao, J. Jing, JHEP **1305**, 101 (2013) [arXiv:1306.0064].
- [25] S. Gangopadhyay, D. Roychowdhury, JHEP **05**, 002 (2012) [arXiv:1201.6520];
S. Gangopadhyay and D. Roychowdhury, JHEP **05**, 156 (2012) [arXiv:1204.0673].
- [26] A. Sheykhi, D. Hashemi Asl, A. Dehyadegari, Phys. Lett. B **781**, 139 (2018) [arXiv:1803.05724].
- [27] A. Sheykhi, A. Ghazanfari, A. Dehyadegari, Eur. Phys. J. C **78**, 159 (2018) [arXiv:1712.04331].
- [28] Z. Zhao, Q. Pan, S. Chen and J. Jing, Nucl. Phys. B **871**, 98 (2013) [arXiv:1212.6693].
- [29] Y. Liu, Y. Gong and B. Wang, JHEP **1602**, 116 (2016) [arXiv:1505.03603].

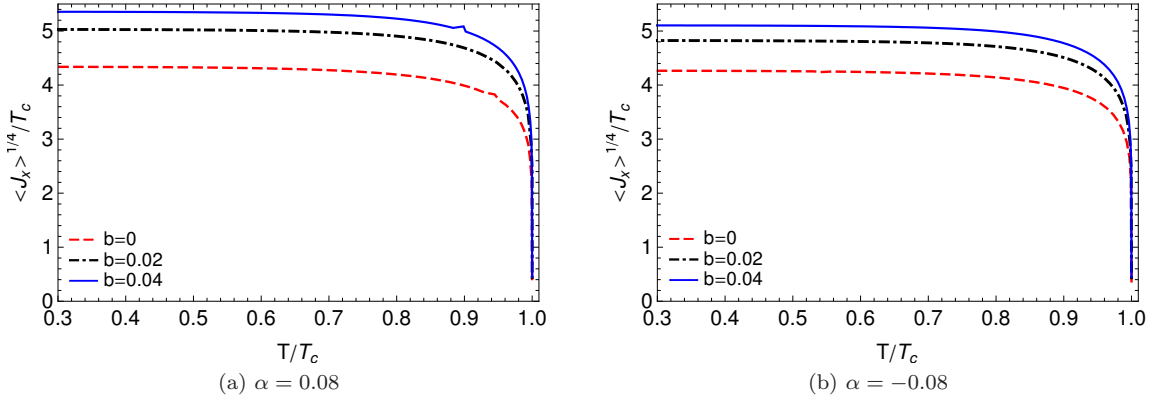


FIG. 16: The behavior of the condensation parameter as a function of the temperature for different values of nonlinearity parameters in $d = 6$ with $\overline{m}^2 = 0$.

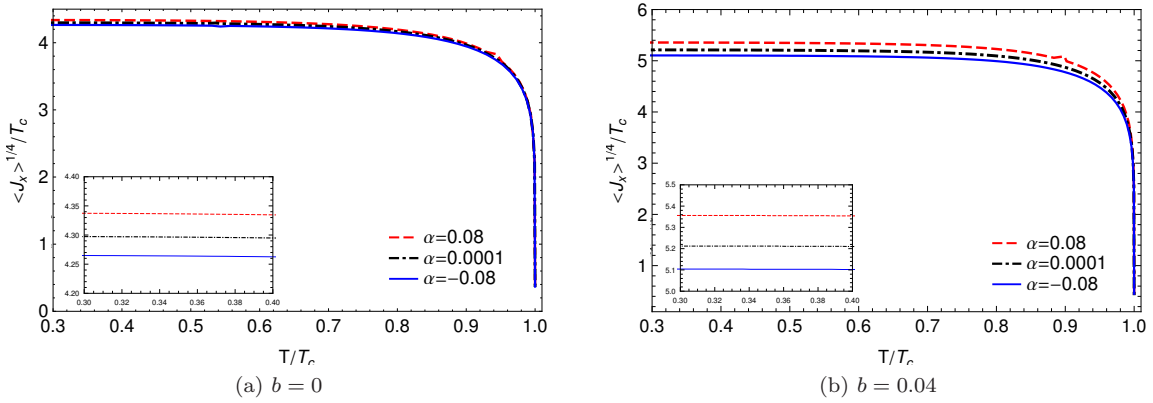


FIG. 17: The behavior of the condensation parameter as a function of the temperature for different values of Gauss-Bonnet parameters in $d = 6$ with $\overline{m}^2 = 0$.

- [30] A. Sheykhi, H. R. Salahi, A. Montakhab, JHEP **1604**, 058 (2016) [arXiv:1603.00075].
- [31] A. Sheykhi, F. Shaker, Int. J. Mod. Phys. D **26**, 1750050 (2017) [arXiv:1606.04364].
- [32] A. Sheykhi, F. Shaker, Can. J. of Phys. **94**, 1372 (2016) [arXiv:1601.05817].
- [33] A. Sheykhi, F. Shaker, Phys Lett. B **754**, 281 (2016) [arXiv:1601.04035].
- [34] S. I. Kruglov [arXiv:1801.06905].
- [35] M. Mohammadi, A. Sheykhi and M. Kord Zangeneh, Eur. Phys. J. C **78**, 654 (2018) [arXiv:1805.07377v1].
- [36] J. Bardeen, L. N. Cooper, J. R. Schrieffer, Theory of Superconductivity, Phys. Rev. **108**, 1175 (1957).
- [37] A.P. Mackenzie, Y. Maeno, Physica B **280**, 148 (2000).
- [38] R.-G. Cai, S. He, L. Li, and L.F. Li, JHEP, **1312**, 036 (2013).
- [39] R.G.Cai, L. Li, L.F. Li, JHEP, **1401**, 032 (2014) [arXiv:1309.4877v3].
- [40] A. Donos and J.P. Gauntlett, JHEP **12**, 091 (2011).
- [41] S. S. Gubser and S. S. Pufu, JHEP, **0811**, 033 (2008).
- [42] P. Chaturvedi, G. Sengupta, JHEP, **1504**, 001 (2015) [arXiv:1501.06998v1].
- [43] M. M. Roberts and S. A. Hartnoll, JHEP **0808**, 035 (2008) [arXiv:0805.3898].
- [44] H. B. Zeng, W. M. Sun and H. S. Zong, Phys. Rev. D **83**, 046010 (2011) [arXiv:1010.5039 [hep-th]].
- [45] R. G. Cai, Z. Y. Nie and H. Q. Zhang, Phys. Rev. D **83**, 066013 (2011) [arXiv:1012.5559].
- [46] L. A. Pando Zayas and D. Reichmann, Phys. Rev. D **85**, 106012 (2012) [arXiv:1108.4022].
- [47] D. Momeni, N. Majd and R. Myrzakulov, Europhys. Lett. **97**, 61001 (2012) [arXiv:1204.1246].
- [48] S. Gangopadhyay, D. Roychowdhury, JHEP **08**, 104 (2012) [arXiv:1207.6505v2].
- [49] M. Mohammadi, A. Sheykhi and M. Kord Zangeneh, Eur. Phys. J. C **78**, 984 (2018) [arXiv:1901.10540].
- [50] F. Benini, C. P. Herzog, R. Rahman and A. Yarom, JHEP **1011**, 137 (2010) [arXiv:1007.1981].
- [51] F. Benini, C. P. Herzog and A. Yarom, Phys. Lett. B **701**, 626 (2011) [arXiv:1006.0731].
- [52] R. G. Cai, Z. Y. Nie and H. Q. Zhang, Phys. Rev. D **82**, 066007 (2010) [arXiv:1007.3321v2].
- [53] J. W. Lu, Y. B. Wu, T. Cai, H. M. Liu, Y. S. Ren and M. L. Liu, Nucl. Phys. B **903**, 360 (2016).
- [54] S. H. Hendi, JHEP **03**, 065 (2012).

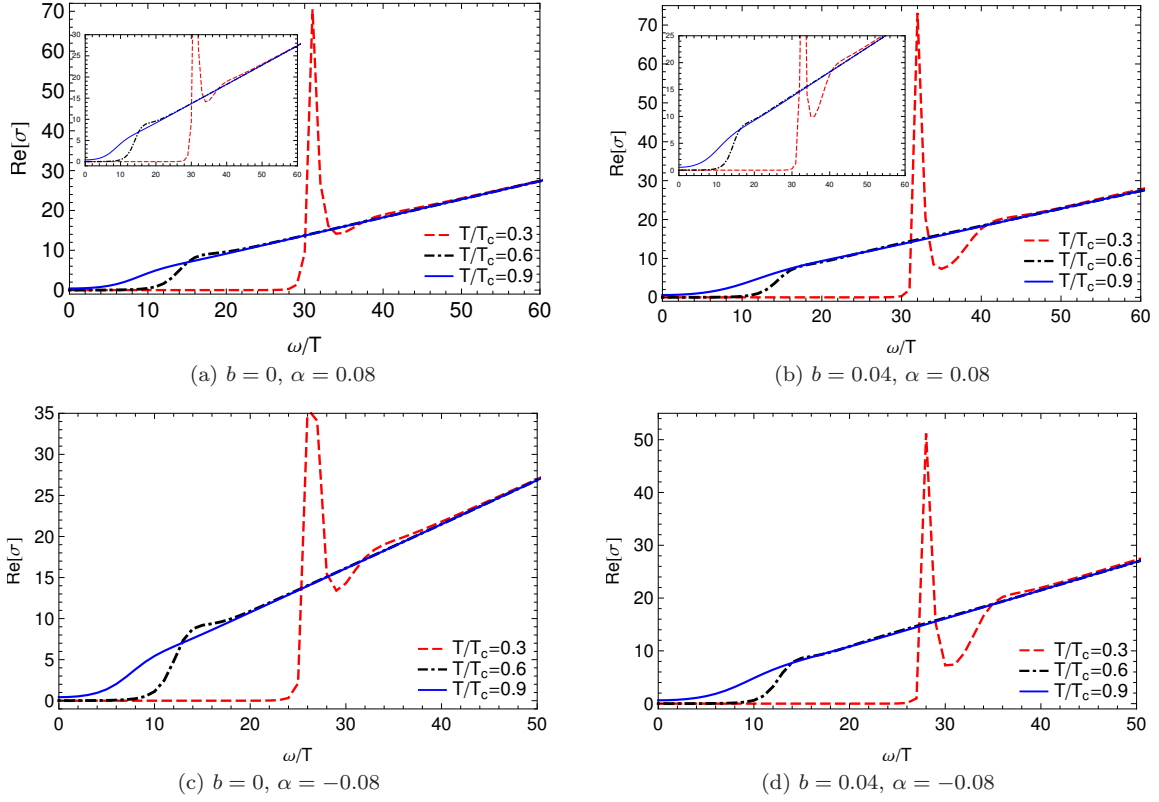


FIG. 18: The behavior of real parts of conductivity with $\overline{m}^2 = -3/4$ in $d = 5$.

- [55] A. Ritz and R. Delbourgo, Int. J. Mod. Phys. A **11**, (1996) 253 [hep-th/9503160].
- [56] J.T. Liu and P. Szepietowski, Phys. Rev. D **79**, 084042 (2009) [arXiv:0806.1026].
- [57] Y. Kats, L. Motl and M. Padi, JHEP **12**, 068 (2007) [hep-th/0606100].
- [58] D. Anninos and G. Pastras, JHEP **07**, 030 (2009), [arXiv:0807.3478].
- [59] D. Wen, H. Yu, Q. Pan, K. Lin and W. L. Qian, Nucl. Phys. B **930**, 255 (2018) [arXiv:1803.06942v2].
- [60] K. Skenderis, Quant. Grav. **19**, 5849 (2002), [arXiv:hep-th/0209067].
- [61] M. Brigante, H. Liu, R. C. Myers, S. Shenker and S. Yaida, Phys. Rev. D **77**, 126006 (2008) [arXiv:0712.0805 [hep-th]].
- [62] M. Brigante, H. Liu, R. C. Myers, S. Shenker and S. Yaida, Phys. Rev. Lett. **100**, 191601 (2008) [arXiv:0802.3318 [hep-th]].
- [63] A. Buchel and R. C. Myers, JHEP **0908**, 016 (2009) [arXiv:0906.2922 [hep-th]].
- [64] D. M. Hofman, Nucl. Phys. B **823**, 174 (2009) [arXiv:0907.1625 [hep-th]].
- [65] J. de Boer, M. Kulaxizi and A. Parnachev, JHEP **1003**, 087 (2010) [arXiv:0910.5347 [hep-th]].
- [66] X. O. Camanho and J. D. Edelstein, JHEP **1004**, 007 (2010) [arXiv:0911.3160 [hep-th]].
- [67] A. Buchel, J. Escobedo, R. C. Myers, M. F. Paulos, A. Sinha and M. Smolkin, JHEP **1003**, 111 (2010) [arXiv:0911.4257 [hep-th]].

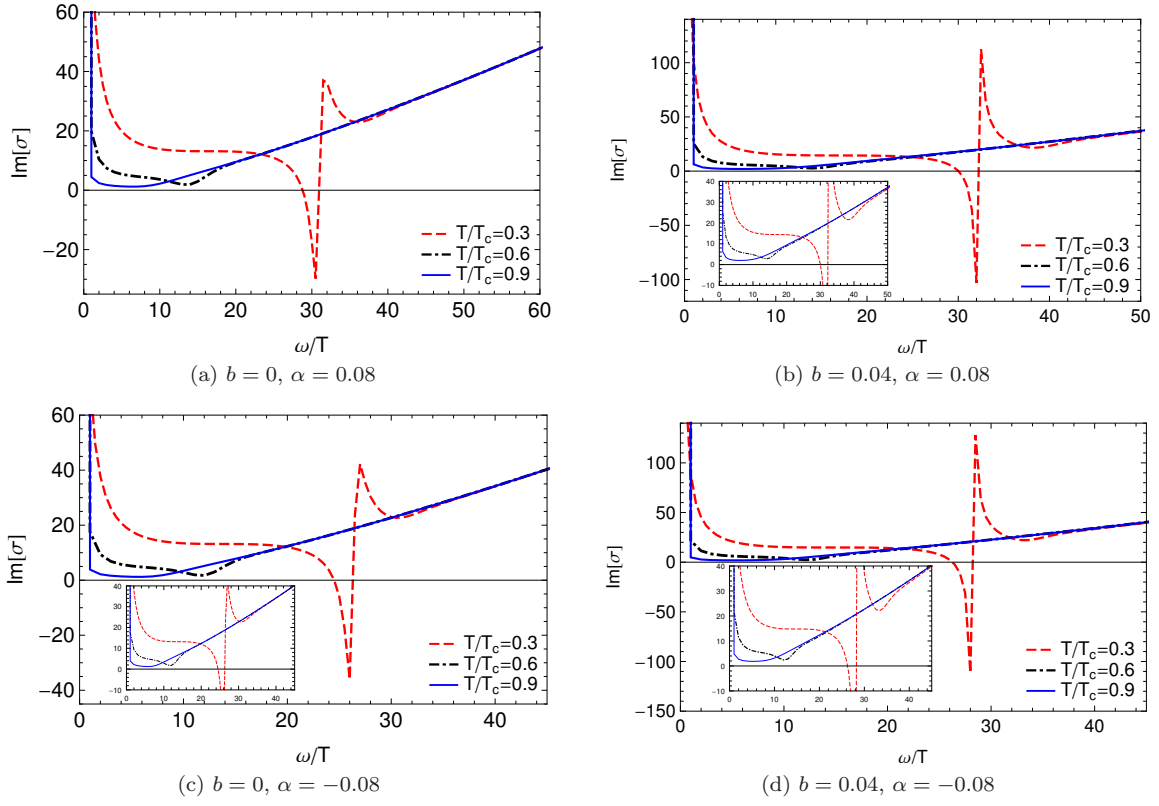


FIG. 19: The behavior of imaginary parts of conductivity with $\overline{m}^2 = -3/4$ in $d = 5$.

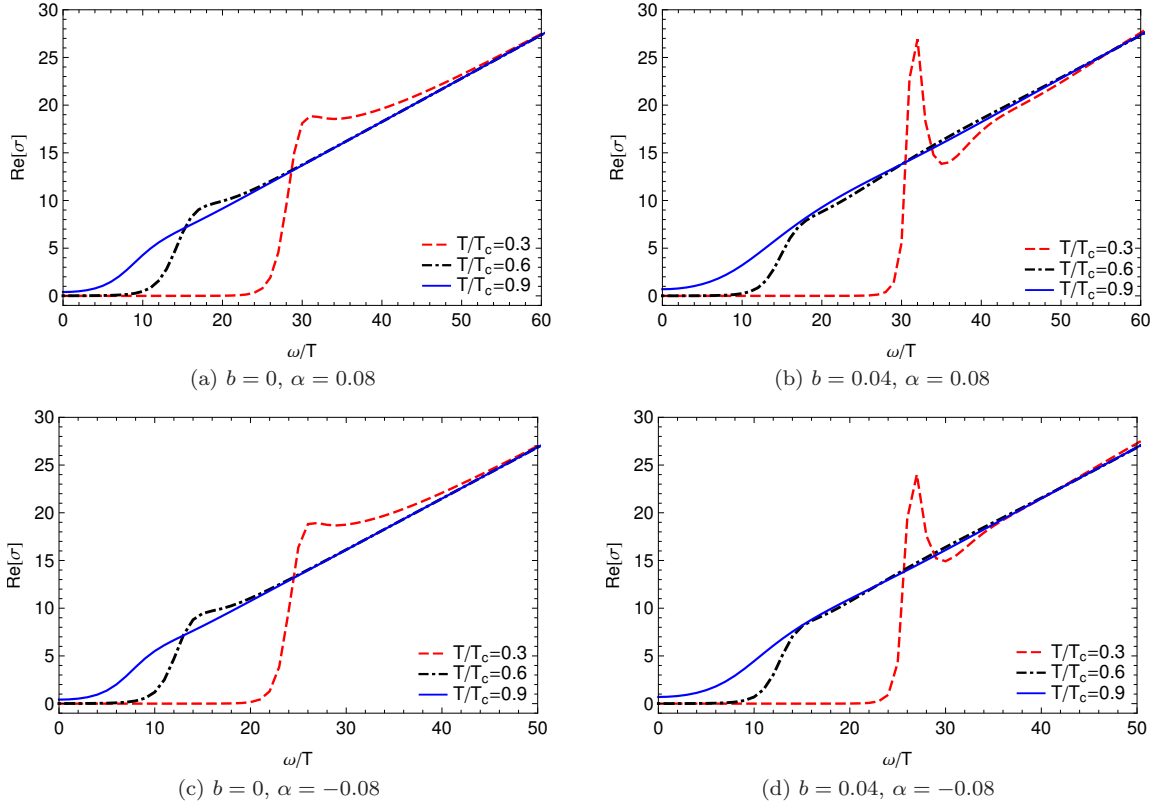


FIG. 20: The behavior of real parts of conductivity with $\overline{m}^2 = 0$ in $d = 5$.

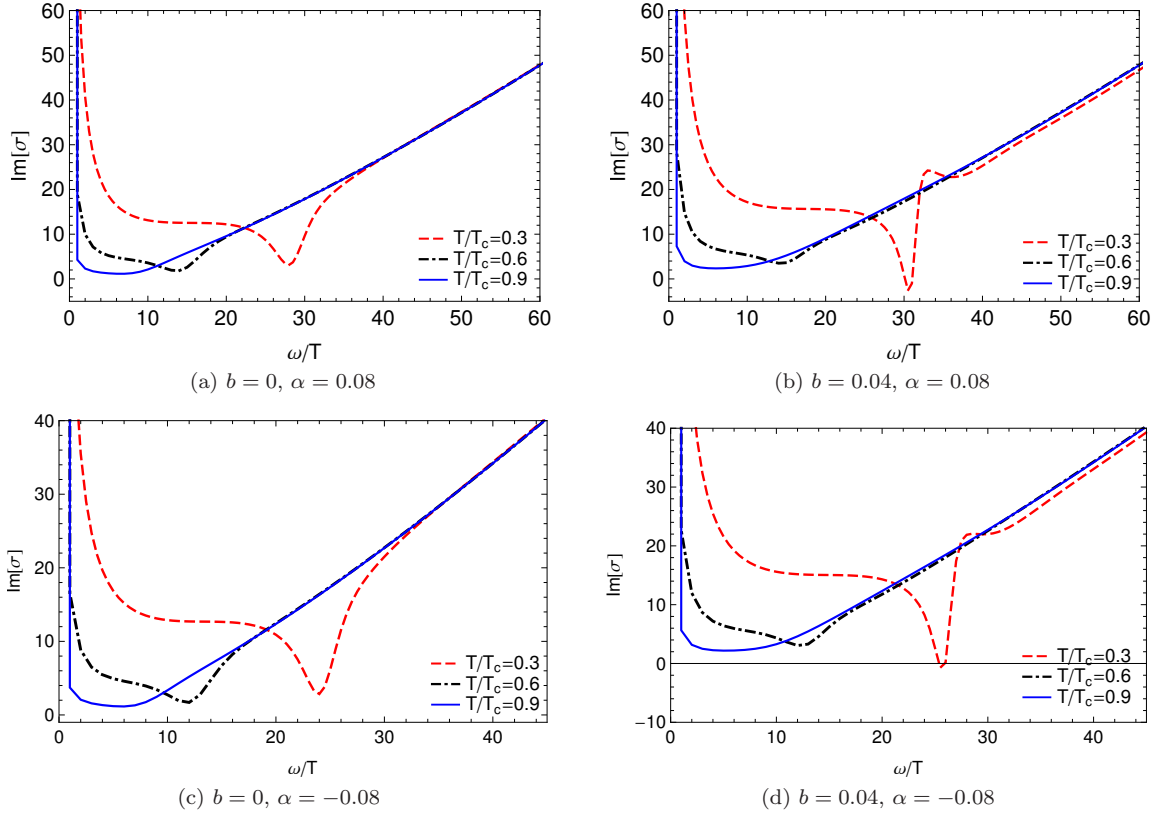


FIG. 21: The behavior of imaginary parts of conductivity with $\overline{m}^2 = 0$ in $d = 5$

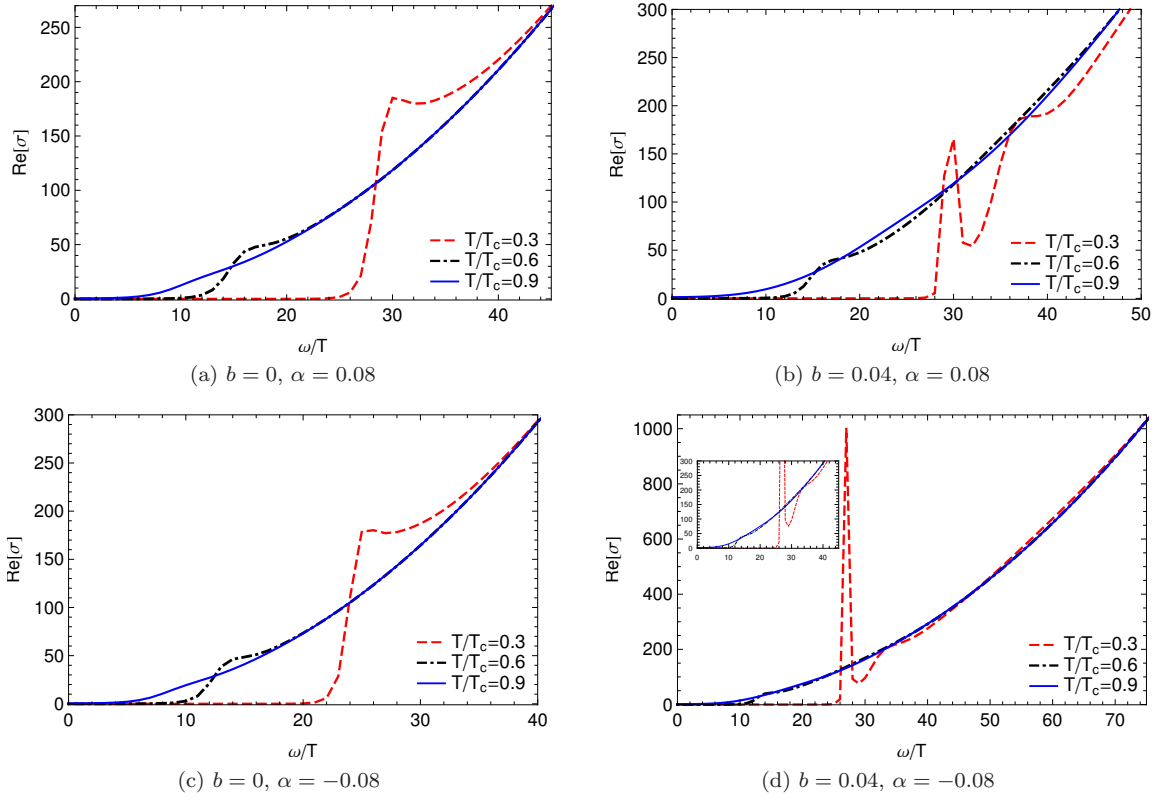


FIG. 22: The behavior of real parts of conductivity with $\overline{m}^2 = 0$ in $d = 6$

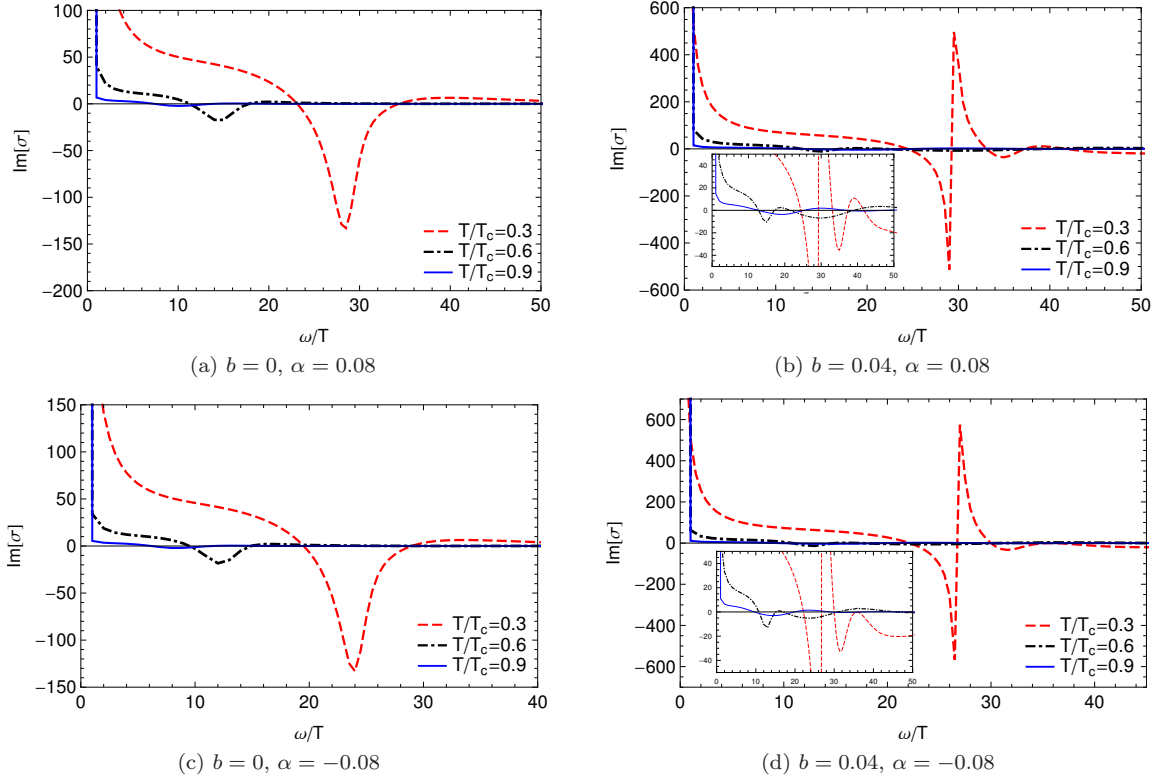


FIG. 23: The behavior of imaginary parts of conductivity with $\overline{m}^2 = 0$ in $d = 6$.

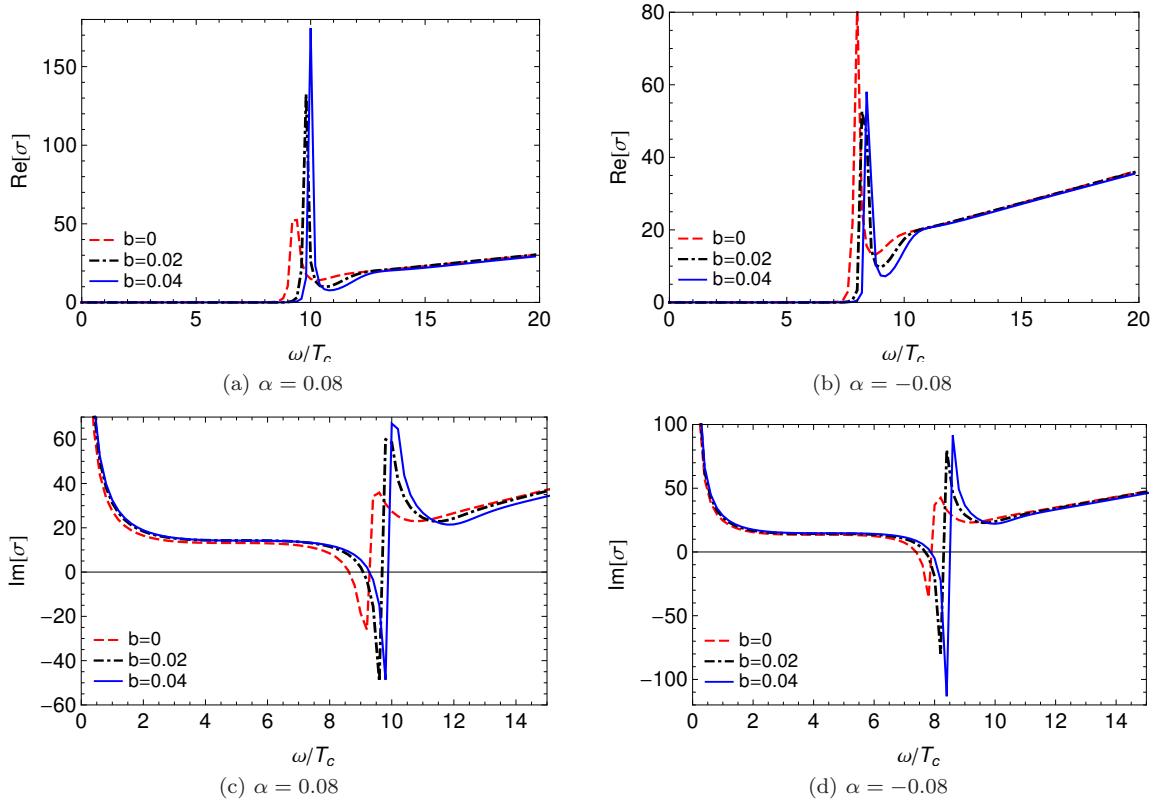


FIG. 24: The behavior of real and imaginary parts of conductivity with $\overline{m}^2 = -3/4$ and $T/T_c = 0.3$ in $d = 5$.

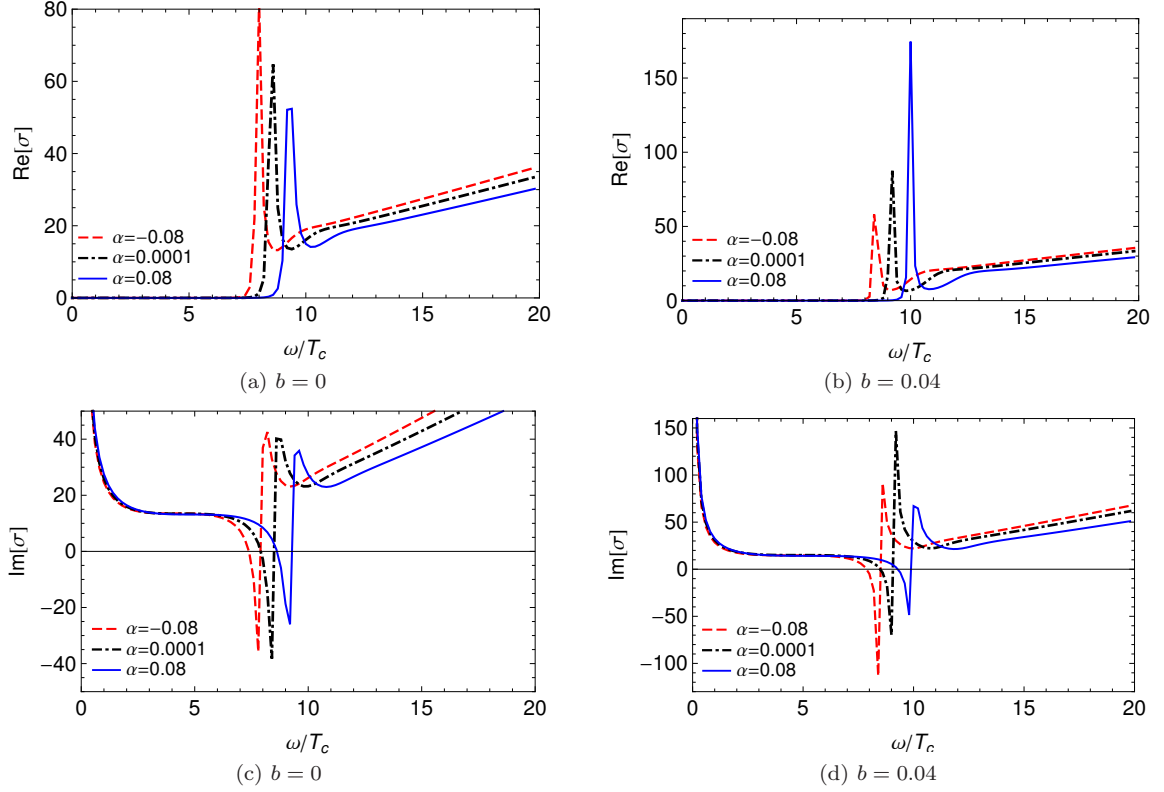


FIG. 25: The behavior of real and imaginary parts of conductivity for $\overline{m}^2 = -3/4$ and $T/T_c = 0.3$ in $d = 5$.

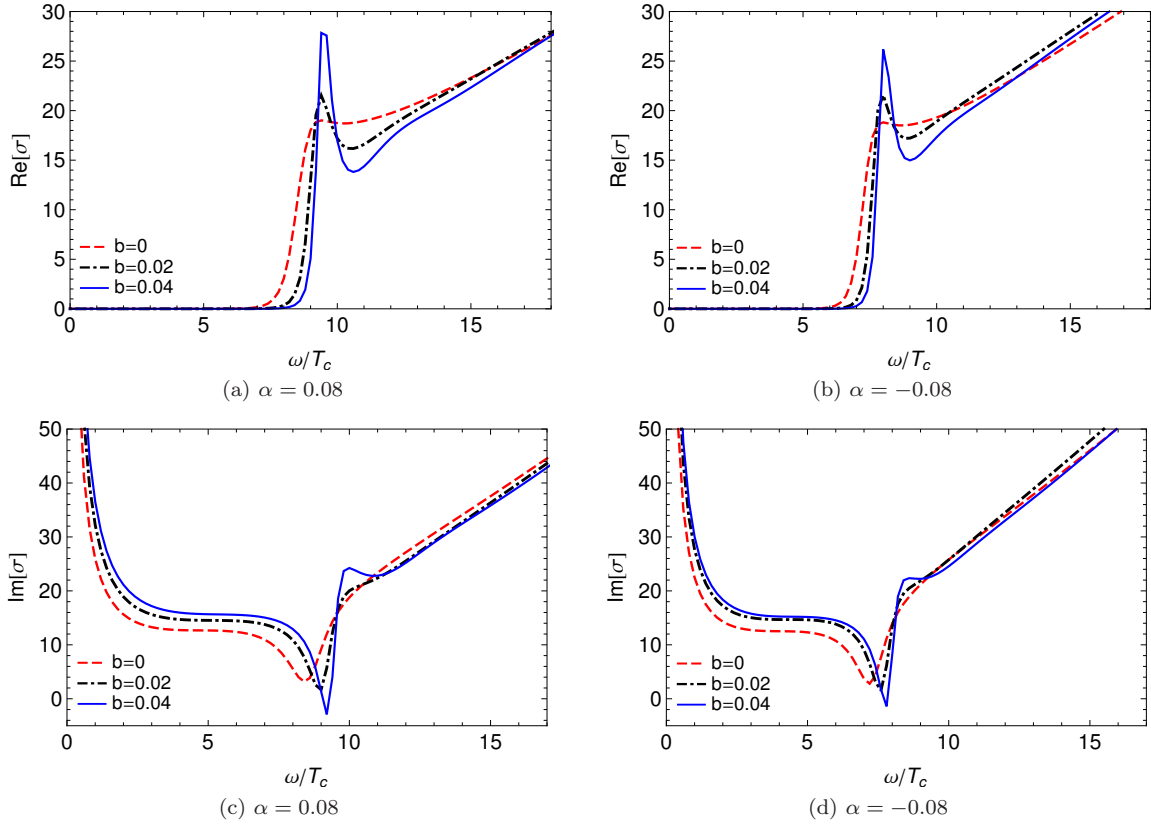


FIG. 26: The behavior of real and imaginary parts of conductivity for $\overline{m}^2 = 0$ and $T/T_c = 0.3$ in $d = 5$.

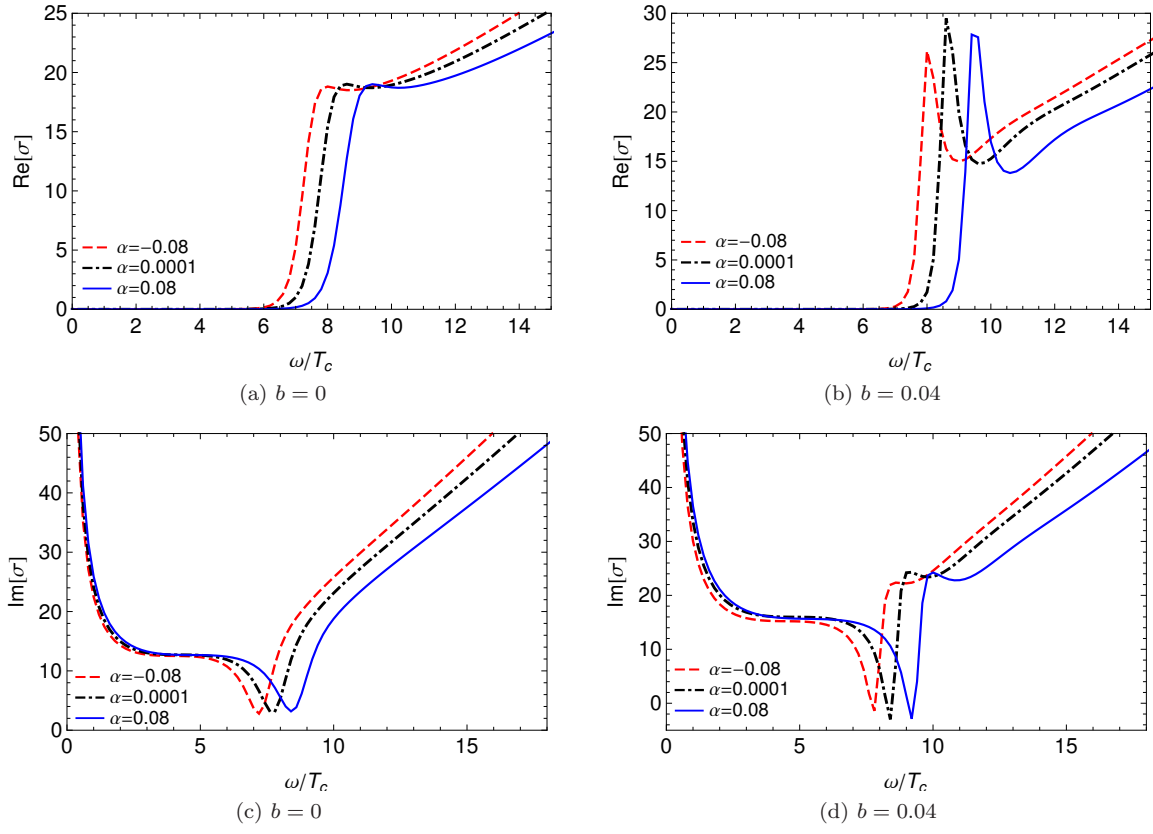


FIG. 27: The behavior of real and imaginary parts of conductivity for $\overline{m}^2 = 0$ and $T/T_c = 0.3$ in $d = 5$.